Australian Government
Department of Defence
Defence Science and
Technology Organisation

Generic Design Procedures for the Repair of Acoustically Damaged Panels

R.J. Callinan, C.H. Wang, S. Sanderson and S.C. Galea

Air Vehicles Division
Defence Science and Technology Organisation

DSTO-RR-0283

ABSTRACT

Acoustic fatigue is the result of high frequency lateral vibration of an aircraft panel due to time varying pressure waves caused by engine and / or aerodynamic effects. For example, acoustically induced cracks have been recorded in the lower external surface of the nacelle skin of the F / A-18 aircraft and aft fuselage. In the case of the inlet nacelle overall sound pressure levels of the order of 172 dB have been recorded. Attempts to repair these cracks by applying standard methods of bonded repair developed for in-plane loads were made. However, the cracks continued to grow at a similar rate. While the repair of cracked aircraft structures subjected to in-plane loads using bonded repairs has resulted in considerable aircraft life time extension and hence cost savings, the use of bonded patches to repair panels with acoustically induced cracks (acoustic fatigue) is only recent. In this report a generic design procedure is presented for the repair of panels containing acoustically induced cracks using constrained layer damping (CLD). The application of bonded repairs to acoustically-induced cracks requires analytical tools that take into account high frequency out-of-plane vibration. The analytical tools described in the report will enable the rapid design of effective repairs using closed form solutions. A potential outcome for this study could be application to the repair of the batch 11 F / A-18 aircraft which suffer from acoustic fatigue cracking on the aft fuselage. Over a period of ten years this could result in cost savings of one order of magnitude improvement over those for metallic repairs.

Published by

Air Vehicles Division
DSTO Defence Science and Technology Organisation
506 Lorimer St
Fishermans Bend, Victoria 3207 Australia

Telephone: (03) 9626 7000
Fax: (03) 9626 7999

AR-013-231
December 2008

APPROVED FOR PUBLIC RELEASE

Generic Design Procedures for the Repair of Acoustically Damaged Panels

Executive Summary

Currently a batch of eleven RAAF F/A-18 aircraft are developing acoustic fatigue cracks in the rear fuselage area as a result of high frequency lateral vibrations due to time varying pressure waves caused by engine and/or aerodynamic effects. The repair of cracked aircraft structures subjected to in-plane loads using bonded repairs has resulted in considerable aircraft life time extension and hence cost savings. However, the use of bonded patches to repair panels with acoustically induced cracks (acoustic fatigue) is a recent development. In this report, a generic design procedure is described for the repair of panels containing acoustically induced cracks. This procedure consists of a simplified dynamic analysis together with crack bridging theory. Furthermore, the solution is also applicable for plates containing cracks on the boundary. In addition the procedure makes use of a closed form solution to determine the effect of residual thermal stresses and softening of the adhesive. It has been shown that the analysis for crack bridging can predict the behaviour of plates simply supported on all edges or clamped edges.

The generic design procedure models the viscoelastic damping material and boron/epoxy constraining layer in order to damp out vibration of the panels. As a result this generic design procedure together with damping data will aid in the design of highly damped repairs to acoustically-induced cracked panels. The generic design procedure has been validated using finite element analysis. The goal of this work is eventually to incorporate the design method into the RAAF Engineering Standard DEF(AUST)9005-A, to enable rapid design of such repairs.

It has been found that the use of a highly damped repair is a low risk, low cost repair that could be used on the aft fuselage of the F/A-18 to extend the life of this component beyond 6000 hours. Furthermore over a period of 10 years, the cost savings are an order of magnitude improvement over those for metallic repairs.

Authors

R.J. Callinan
Air Vehicles Division

Mr. R.J.Callinan is a senior research scientist and graduated from RMIT (Aero. Eng.) in 1969 and from Monash University in 1971 (Civil. Eng.) and completed a M.Eng. Sc. in 1981 at Melbourne University. His work has been in the areas of finite element analysis, fracture mechanics and structural mechanics of composite and bonded repairs and military aircraft accident investigations. He has also been involved with design studies of low radar cross-section battlefield surveillance R.P.V.'s. In 1985 he was seconded to the USAF at Eglin AFB for 18 months, to carry out vulnerability studies on composite structures. More recently he has been involved in a specific program on validation of bonded repairs to RAAF aicraft, and bonded repairs subject to acoustic fatigue.

C.H. Wang
Air Vehicles Division

Chun Wang is currently a principal research scientist and Functional Head of composite and low-observable structures in the Air Vehicles Division. He has a PhD in Mechanical Engineering from the University of Sheffield, UK. Prior to joining DSTO in 1995, he had worked at various universities in the UK and Australia as research fellow and lecturer. His main research expertise is in the areas of fatigue and fracture mechanics, composite structures, bonded structural repairs, propagation and scattering of acoustic and electromagnetic waves.

S. Sanderson
Air Vehicles Division

Mr. Sanderson commenced work at the Aeronautical Research Laboratory in 1981. He has developed flight data reduction and analysis software for Mirage, F-111 and F/A-18 projects. Several of these programs have been implemented by NAE for part of their data reduction in the IFOSTP project. Since 1992, Mr. Sanderson has undertaken finite element analysis of composite and bonded structures for the F-111 and F/A-18 aircraft and provided training in finite element modelling and analysis. In 1998 Mr. Sanderson was appointed as the Systems Administrator of the Air Vehicles Division Computational Structural Analysis Facilities.

Dr S.C. Galea
Air Vehicles Division

Dr Galea graduated in 1980 with a Bachelor of Engineering (Mech) from the University of Queensland with first class honours and in 1983, he received a Masters of Engineering Science. He commenced employment with the Aeronautical Research Laboratory in 1983. In 1985 he commenced studies at the Institute of Sound and Vibration Research, University of Southampton, UK and received his Doctor of Philosophy from the University of Southampton in 1989. Dr Galea is currently a Principal Research Scientist and Functional Head of the Smart Structures and Advanced Diagnostics Group. His current responsibilities involve the management of research and providing technical leadership on the development and application of smart materials and structures technologies to aircraft structures, including in-situ structural health monitoring and self-powering techniques. He has an extensive publication record of over 80 publications, which include three book chapters on smart structures and repairs to acoustically-fatigue structures. Dr Galea is a member of the Editorial Board on the International Journal of Structural Health Monitoring and is the section editor of the Aerospace Applications section in the Encyclopaedia of Structural Health Monitoring. He is also on the Management Steering Committee for the DSTO Key Initiative on Smart Structures and Materials and on the Advisory Board of the ARC Centre for Complex Dynamic Systems and Control.

Contents

Symbols

CLD	Constrained layer damping
C_f	Coefficient for crack growth law
D	Bending stiffness of plate
D_t	Overall bending stiffness of 3 layer plate
E	Overall Young's modulus
E_1	Young's modulus for plate
$E_1^{'}$	Real part of complex Young's modulus for plate
E_3	Young's modulus for constraining layer
$E_3^{'}$	Real part of complex Young's modulus for constraining layer
F	Geometry factor, for location on panel
G	Shear modulus for damping layer
G_a	Shear modulus for adhesive
G'_2	Real part of complex shear modulus
I_1	Second moment of area of component 1
I_3	Second moment of area of component 3
I_t	Second moment of area for total bending stiffness
I_{tr}	Second moment of area for real part of bending stiffness
L_x	Length of plate in x direction
L_y	Length of plate in y direction
L	Load alleviation factor
K	Stress intensity factor
K_f	Constant for crack growth law
K_u	Stress intensity factor un-patched
K_p	Stress intensity factor patched
K_{min}	Minimum stress intensity factor
K_{mean}	Mean stress intensity factor
K_{max}	Maximum stress intensity factor
K_{rms}	Root mean square stress intensity factor
$K_{rms\text{-}u}$	Root mean square stress intensity factor un-repaired
$K_{rms\text{-}r}$	Root mean square stress intensity factor repaired
$(K_{\max})_{rms}$	Maximum rms stress intensity factor
K_T	Stress intensity factor due to thermal stresses
M_{ave}	Average bending moment along crack
$OASPL$	Overall Sound Pressure Level
PSD	Power Spectral Density
R	Ratio of minimum to maximum stress during a load cycle
SPL	Sound pressure level
S_o	Power spectral density of the response
S_i	Power spectral density of the excitation
ΔT	Change from cure to operating temperature
T_c	Cure temperature
T_o	Operating temperature

Y	Geometric factor
W	Geometry factor for frequency
a	Half crack length
d_1	Distance from centroid of overall structure to centre of plate
d_3	Distance from centroid of overall structure to centre of constraining layer
f	Frequency of plate
f_m	Membrane component of the normalized stress intensity factor
f_b	Bending component of the normalized stress intensity factor
f_o	First resonant frequency of the plate
f_c	First resonant frequency of the repaired plate
Δf	Frequency range
g_{opt}	Optimum value of shear parameter
g_m	Geometric shear parameter
g'	Real part complex geometric shear parameter
h	Thickness of plate
h_1	Thickness of plate for component 1
h_2	Thickness of plate for component 2
h_3	Thickness of plate for component 3
h_{13}	Distance from centroid of component 1 to centroid of component 3
k_f	The wave number
k_x	Modal wave number in x direction
k_y	Modal wave number in y direction
m_t	Total mass per unit mass
m	Also denotes coefficient in crack growth law
m	Fundamental mode in *x* direction
n	Fundamental mode in *y* direction
p_{rms}	rms fluctuating pressure
s	Stiffness ratio
t_a	Thickness of adhesive layer
w	Transverse displacement of plate
α	Thermal coefficient of expansion
α_1	Thermal coefficient of expansion for component 1
α_3	Thermal coefficient of expansion for component 3
α_{alum}	Thermal coefficient of expansion for aluminium
α_{boron}	Thermal coefficient of expansion for boron
α_{eff}	Effective coefficient of thermal expansion
β	Moment correction factor for rectangular plate
η	Loss factor
η_s	Loss factor for 3 layer plate
η_c	Loss factor for viscoelastic damping layer
$\eta_{s,\max}$	Optimum loss factor for 3 layer plate
η_1	Loss factors for component 1

η_2	Loss factors for component 2
η_3	Loss factors for component 3
$\mu_{DC,m}$	Modal loss factor
ν	Poissons ratio for plate
ν_1	Poissons ratio for plate component 1
ν_3	Poissons ratio for plate component 3
σ_b	Far field bending stress
σ_m	Far field membrane stress
ρ	Density of plate
ρ_1	Density of plate component 1
ρ_2	Density of damping layer, component 2
ρ_3	Density of constraining layer
ω_M	m^{th} resonant frequency

1. Introduction

The repair of cracked aircraft structures subjected to in-plane loads using bonded repairs has resulted in considerable aircraft lifetime extension and hence cost savings [1]. However, the use of bonded patches to repair panels with acoustically induced cracks (acoustic fatigue) is a recent development. In this report, a generic design procedure for the repair of panels containing acoustically induced cracks will be described. Acoustic fatigue is a result of high frequency lateral vibration in aircraft panels due to time varying pressure waves caused by engine and/or aerodynamic effects. For instance, acoustically induced cracks have been recorded in the lower external surface of the nacelle skin of the F/A-18 aircraft, as shown in Figure 1. In this case, overall sound pressure levels of the order of 172 dB have been reported, [2] and [3]. Attempts were made to repair these cracks by applying standard methods of bonded repair [4] developed for in-plane loads, however, the cracks continued to grow. It was found [5] that while the boron fibre composite bonded repairs did reduce the stress intensity at the crack-tip, the high number of cycles still lead to significant crack growth of up to 2 mm per flight hour. The application of bonded repairs to acoustically-induced cracks requires analytical tools that can take into account high frequency out-of-plane vibration.

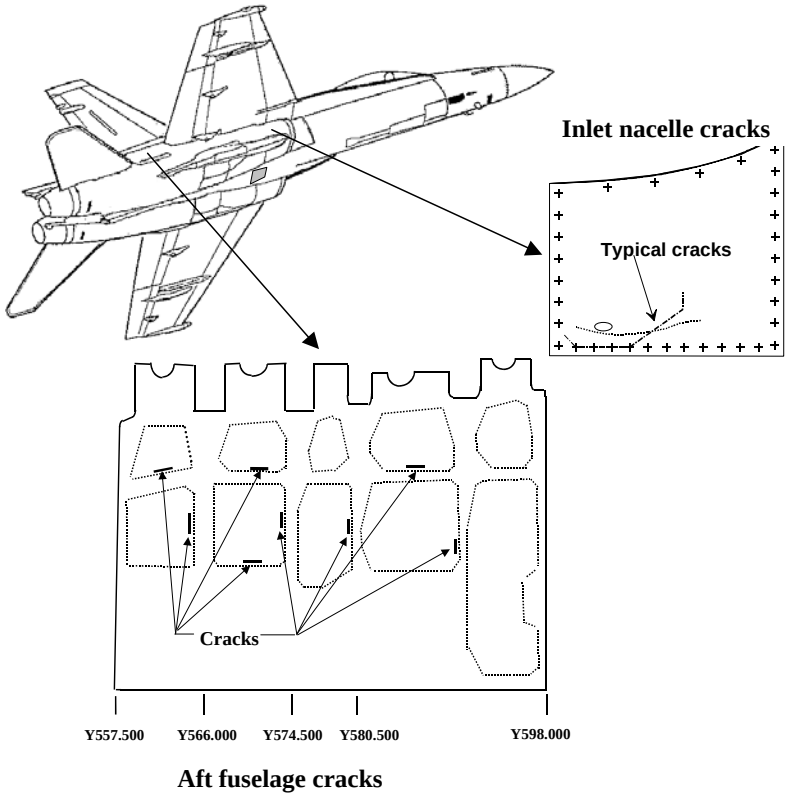

Figure 1: Location of acoustic fatigue cracking in F/A-18 fuselage panels

Since it is known that the amplitude of vibration is inversely proportional to the square root of the damping ratio, a combination of damping and stiffness may reduce the crack growth rate significantly. The application of highly damped repairs (Durability Patches) to acoustically

damaged panels has been proposed by Rogers *et al* [6]. Also, a highly damped repair was applied [7] to the vertical fin of the F-15 aircraft, as part of a test program. (More recently, a series of repairs have been designed and tested in the AFRL progressive wave tunnel [8, 9]). Also Boeing [10] have developed procedures for the use of the Dosimeter, and methods for optimal design of damped repairs. Repairs have been made to B52 fuselage skin panels, F-15 access panel and C130 flap panels, and the Dosimeter has been used for the assessement of the effectiveness of the repair [10]. The Dosimeter being a small autonomous device, carried in an aircraft, and designed to measure the thermo-acoustic environment of an aircraft skin plate.

In this report, a generic design procedure (based on constrained layer damping (CLD)) will be presented. This will involve the selection of a damping material and the geometry of the CLD in order to prevent the growth of acoustically-induced cracks. This work makes use of the closed form solution for the stress intensity factor developed by DSTO [11].

2. Overview of design procedure

The use of CLD containing a viscoelastic material is well known and is an effective method of dissipating the energy due to flexural vibration. As shown in Figure 2, CLD involves a plate, viscoelastic material and a constraining layer. In the present context, the constraining layer is effectively the repair patch. The bending of the structure involves shear deformation of the viscoelastic material. Damping occurs since the viscoelastic material is a polymer comprised of long chain molecules which when deformed results in friction of these molecules. A measure of the effectiveness of the CLD is the loss factor, η. For a vibrating plate, the loss factor may be defined as the ratio of the energy dissipated per radian to the total strain energy. The viscoelastic material has a very high loss factor in comparison to metallic components. Also the constraining layer should be very stiff in order to promote shear deformation of the viscoelastic material, i.e. the use of boron / epoxy.

It is known that the amplitude of vibration is inversely proportional to the square root of the loss factor. Hence the higher the loss factor the lower the amplitude of vibration or stress in the plate. Shown in Figure 3 is a plot of shear modulus and loss factor versus temperature for a viscoelastic damping material. Three distinct states exist, namely, glassy, transition and rubbery. The maximum loss factor occurs in the transition state. It is evident that these viscoelastic damping materials are optimum over a limited temperature range. The response is also dependent on the frequency. Hence the correct material must be used for the expected environment (temperature and resonant frequency). The material response for different damping materials is considered in Section 3.

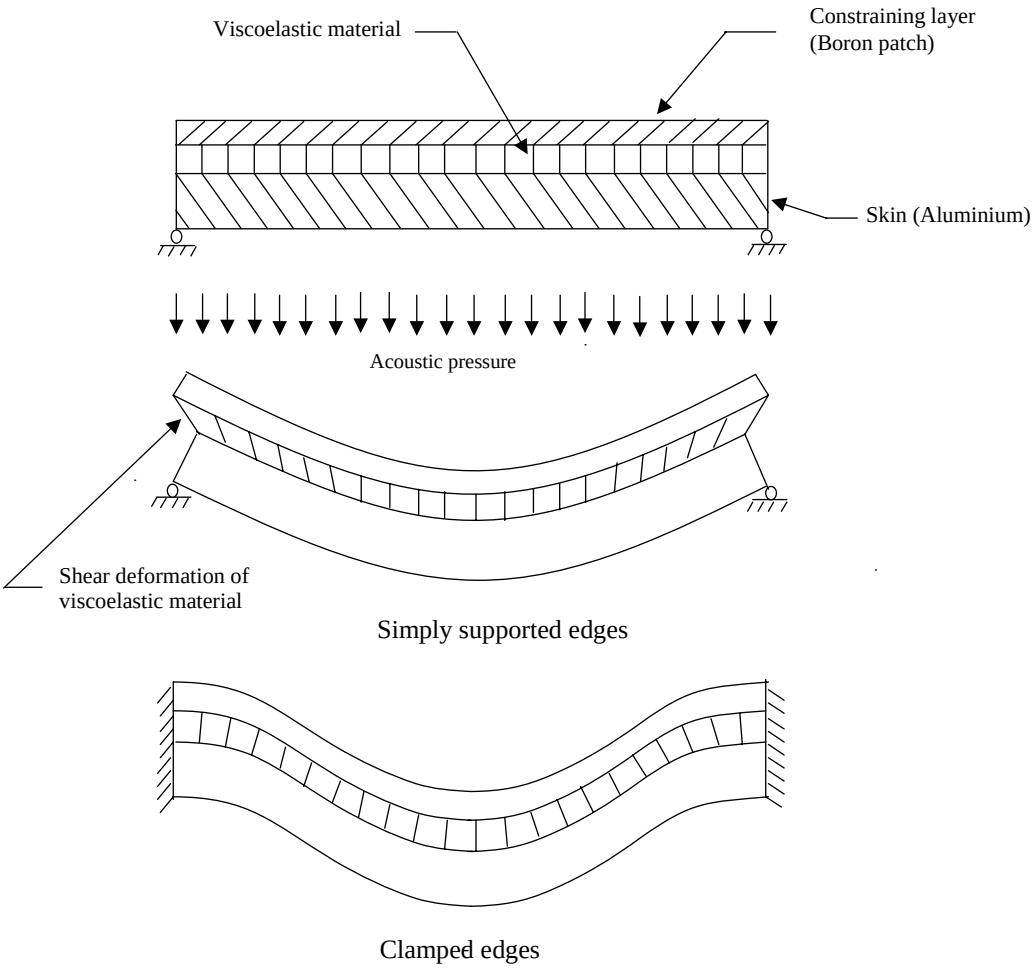

Figure 2: Shear deformation of viscoelastic layer under constrained layer damping

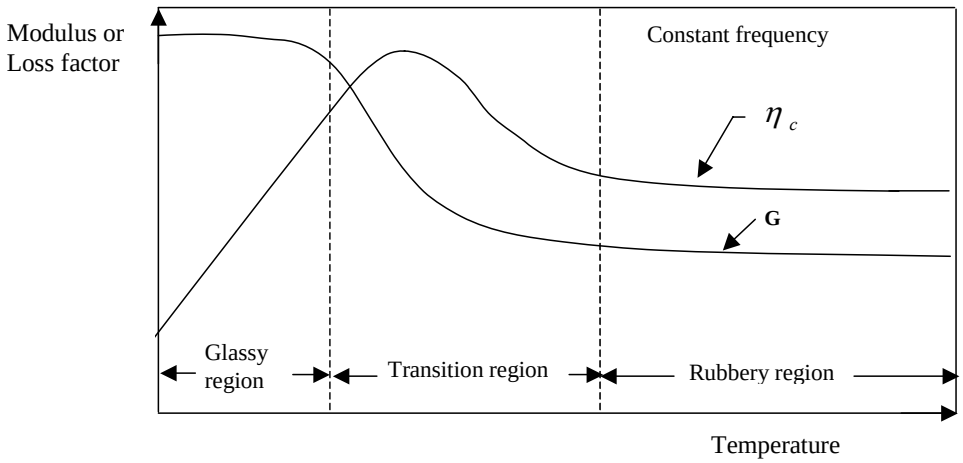

Figure 3: Plot of shear modulus and loss factor as a function of temperature at constant frequency for a viscoelastic material

To simplify the 3D analysis of damped repairs, an analytical solution to a three- layered plate will be considered in order to obtain the loss factor and the resonant frequency. Consider a rectangular plate as shown in Figure 4 with a single viscoelastic layer and a constraining layer with simply supported edges. The moduli of elasticity of the plate and the constraining layer are E_1 and E_3 respectively, and the damping layer is characterized by its shear modulus G_2. Hence the flexural stiffness of layers 1 and 3 are E_1I_1 and E_3I_3, where I_1 and I_3 are the second moment of area of the cross-sections of layer 1 and 3 respectively.

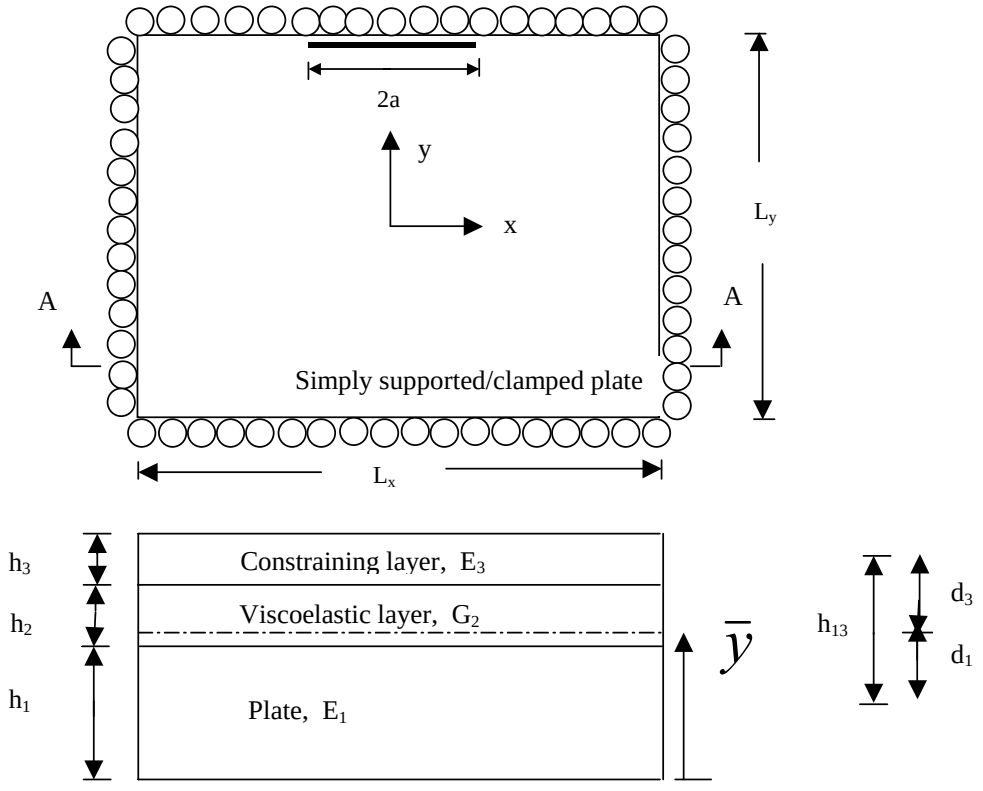

Figure 4: Geometry for constrained layer damping of a simply supported plate

Let the plate lie in the x-y plane, then the governing equation of the displacement, w, in the z direction is given by [p386, 12]:

$$EI_t \frac{\partial^6 w}{\partial x^6} - g^* EI_s \frac{\partial^4 w}{\partial x^4} + m_t \left[\frac{\partial^4 w}{\partial x^2 \partial t^2} - g^* \frac{\partial^2 w}{\partial t^2} \right] = \frac{\partial^2 p(x,t)}{\partial x^2} - g^* p(x,t) \qquad (1)$$

where $p(x,t)$ is space-time-dependent acoustic pressure, g^* is the complex shear parameter (defined later) and m_t is the total mass per unit length of the beam. The bending stiffness terms are

$$EI_t = E_1 I_1 + E_3 I_3 \qquad (2)$$

$$EI_s = EI_t (1+Y) \qquad (3)$$

with the geometric factor Y [p389, 12] being

$$Y = \frac{h_{13}^2}{D_t(1-\nu^2)}\left(\frac{E_1 h_1 E_3 h_3}{E_1 h_1 + E_3 h_3}\right). \tag{4}$$

The solution of this equation leads to the explicit relationship for the loss factor for a three layer plate given by [p389, 12],

$$\eta_S = \frac{g_m \eta_c Y}{1 + g_m(2+Y) + g_m^2(1+\eta_c^2)(1+Y)}, \tag{5}$$

where g_m is the geometric shear parameter and η_c is the loss factor for the viscoelastic material. In order to accurately predict the modal loss factor, particularly at low temperatures when the loss factor of the damping material is low, it has been necessary to modify Mead's solution, [12], to include the loss factor of the skin and the constraining layer.

Denoting the loss factors of the aluminium, the viscoelastic material, and the boron patch as η_1, η_2, and η_3, respectively. The Young's moduli of aluminium (E_1), the shear modulus of the visco-elastic layer (G_2), the Young's modulus of the boron patch (E_3) are then given by

$$E_1 = E_1^{'}(1+i\eta_1) \tag{6}$$

$$G_2 = G_2^{'}(1+i\eta_2) \tag{7}$$

$$E_3 = E_3^{'}(1+i\eta_3) \tag{8}$$

with $E_1^{'}$, $E_3^{'}$, and $g^{'}$ denoting real parts of the complex Young's moduli of the plate, the damping layer, and the shear parameter, respectively. The shear parameter is thus

$$g = \frac{G_2^{'}(1+i\eta_2)}{h_2}\left(\frac{1}{E_1^{'}(1+i\eta_1)h_1} + \frac{1}{E_3^{'}(1+i\eta_3)h_3}\right) = g^{'}(1+i\eta_S) \tag{9}$$

where

$$\eta_S = \mathrm{Im}\left[\frac{1+i\eta_2}{E_1^{'}(1+i\eta_1)h_1} + \frac{1+i\eta_2}{E_3^{'}(1+i\eta_3)h_3}\right] / \mathrm{Re}\left[\frac{1+i\eta_2}{E_1^{'}(1+i\eta_1)h_1} + \frac{1+i\eta_2}{E_3^{'}(1+i\eta_3)h_3}\right] \tag{10}$$

The above expression leads to:

$$\eta_S = \frac{E_1 h_1(\eta_2-\eta_3)(1+\eta_1^2) + E_3 h_3(\eta_2-\eta_1)(1+\eta_3^2)}{E_1 h_1(1+\eta_2\eta_3)(1+\eta_1^2) + E_3 h_3(1+\eta_1\eta_2)(1+\eta_3^2)} \tag{11}$$

It is readily seen that the above solution gives $\eta_S = \eta_2$ when $\eta_1 = \eta_3 = 0$.

The total bending stiffness of the repaired structure is

$$EI_t = E_1 I_1 + E_3 I_3 = E_1^{'}(1+i\eta_1)I_1 + E_3^{'}(1+i\eta_3)I_3 = EI_{tr}(1+i\eta_t) \tag{12}$$

with

$$\eta_t = \frac{E_1^{'} I_1 \eta_1 + E_3^{'} I_3 \eta_3}{E_1^{'} I_1 + E_3^{'} I_3} \tag{13}$$

The *m*th complex frequency, given by Equation (9.52) in ref [12], can be written as

$$\omega_m^2(1+i\eta_{DC,m}) = \frac{EI_{tr}(1+i\eta_t)k_f^2}{m_t}\left[1 + Y\frac{g_m(1+i\eta_S)}{1+g_m(1+i\eta_S)}\right] \tag{14}$$

$$g_m = g^{'} / k_f^2 = \frac{G_2^{'}}{k_f^2 h_2}\left(\frac{1}{E_1 h_1} + \frac{1}{E_3 h_3}\right)\left(1-\nu^2\right) \tag{15}$$

The modal loss factor $\eta_{DC,m}$ is the ratio between the imaginary part and the real part of the expression on the right hand side of the equation (13). The effective wave number k_f will be defined later. After some simplification, the modal loss factor becomes,

$$\eta_{DC,m} = \frac{\eta_t + \eta}{1-\eta_t \eta}, \tag{16}$$

with

$$\eta = \frac{g_m \eta_S Y}{1 + g_m(2+Y) + g_m^2(1+\eta_S^2)(1+Y)}, \tag{17}$$

which is the original solution by Mead, without considering the structural loss due to the aluminium and boron patch.

Since $\eta_t << 1$ for most metallic materials, the modal loss factor is approximately equal to

$$\eta_{DC,m} = \eta_t + \eta \ . \tag{18}$$

Hence the modal loss factor will equal the loss factor due to the skin and constraining layer. A value of η_t for 7075-T6 at room temperature is available from ref.[30] where $\eta = 2\delta$ =0.0106. This will not change significantly with temperature or frequency. For built up aircraft structures the skin damping is enhanced by frictional damping due to fasteners resulting in typical loss factors of the order of 3%.

As indicated the geometric shear factor can be expressed as

$$g = g^{'} / k_f^2 \tag{19}$$

and for two-dimensional structures, the shear parameter is related to the wave numbers in two mutually perpendicular directions, which is defined by

$$k_f^2 = k_x^2 + k_y^2, \tag{20}$$

where the modal wave numbers in the *x* and *y* directions for the fundamental mode given by,

$k_x = \pi / L_x$ for simply supported, $= 2\pi / L_x$ for clamped (21a)

$k_y = \pi / L_y$ for simply supported, $= 2\pi / L_y$ for clamped (21b)

with L_x and L_y being the lengths of the plate in the x and y directions respectively.

It can be shown that for a three-layer beam the optimum loss factor is given by [p392, 12] and is modified:

$$\eta_{S,\max} = \frac{\eta_c Y}{(2+Y) + 2\sqrt{(1+Y)(1+\eta_c^2)}} + \eta_t \tag{22}$$

and an optimum value of the shear parameter exists, and is given by [p392, 12]:

$$g_{opt} = \frac{1}{\sqrt{(1+Y)(1+\eta_c^2)}} \tag{23}$$

If the design is not close to the optimum then consider a change in Y, in particular increase the value of h_3 and / or h_2. There may be an aerodynamic restriction of the value of h_3 such that

the thickness of the repair remains within the boundary layer. Key dimensions, material properties and parameters are shown in Table 1. The geometric shear parameter g_m in equation [12] is a function of the wave number k_f, which in turn is a function of the plate dimensions L_x and L_y.

2.1 Design process

The design process is illustrated in Figure 5. Firstly an initial guess is required for the CLD treatment for the structure. Note that in Figure 5 the sound pressure level (SPL) is required, this will be defined in Section 4. The shear modulus, loss factor, Young's modulus, temperature, frequency and SPL, are required. From these quantities geometric shear factor, geometric factor and loss factor are calculated. It may be useful to first examine the optimality for this geometry. If the design is not optimum, the dimensions of the damping layer can be adjusted by changing h_1, h_2 or h_3. For the first design iteration neglect the optimum. Firstly predict displacement and frequencies. The next step calculates stress intensity due to the SPL and residual thermal stresses. Likely crack growth rates and reductions need to be assessed. The design must be acceptable throughout the entire operating temperature range. It may be necessary to choose an alternative damping material if results are not acceptable. The iterative design process is shown in Figure 5.

Table 1: Design parameters including dimensions, properties and parameters

Physical dimensions (Figure 4)	Material properties	Key parameters
h_1, h_2 , h_3 , h_{13} , L_x , L_y , 2a	E_1 , E_3 , G_2 , v_1 , v_3 , ρ_1 , ρ_2 ρ_3	η_s , η_c , η_t, g_m , k_x , k_y , k_f , f_o , K_{rms} ,Y

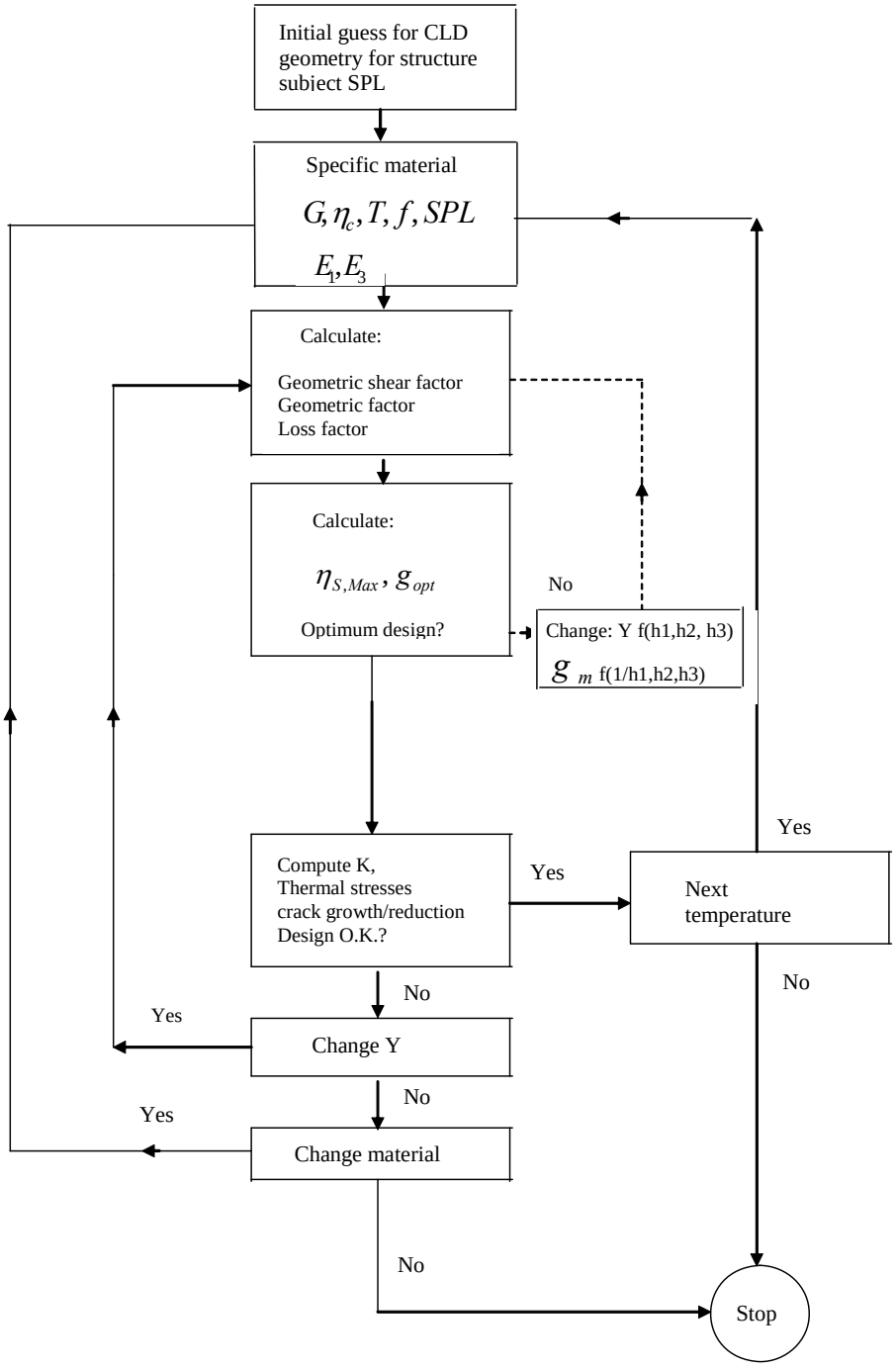

Figure 5: Flow chart for design of highly damped repairs

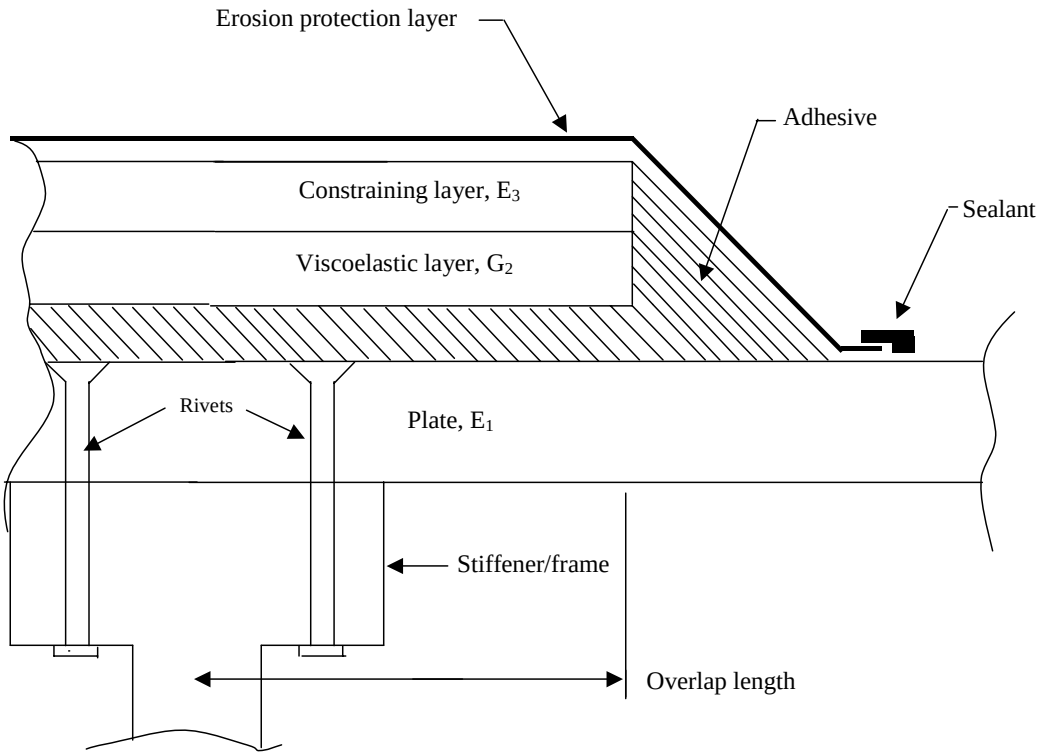

Figure 6: Edge detail necessary to maximise the shear in the viscoelastic layer

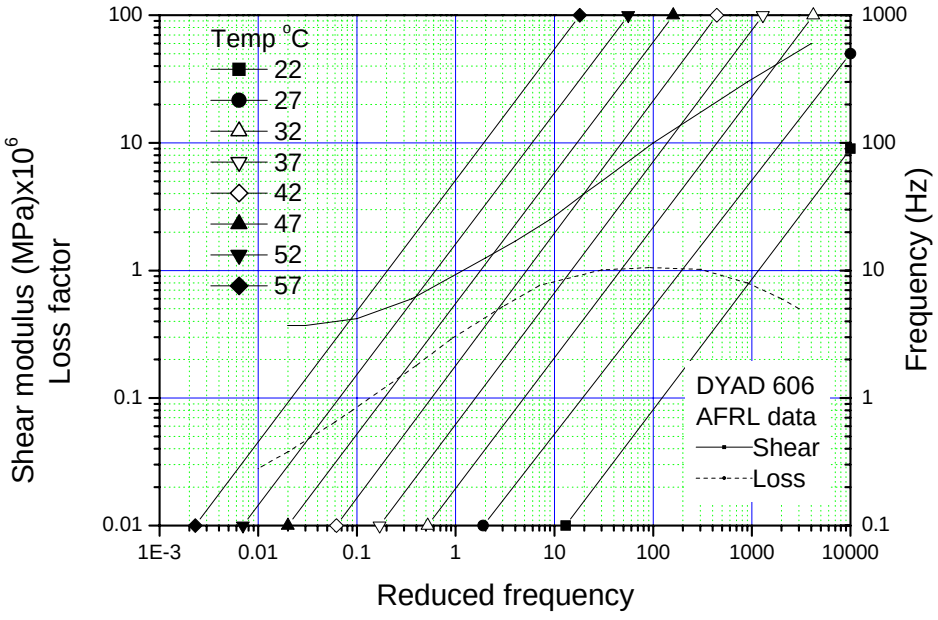

Figure 7: Dyad 606 material data, [14]. (To obtain shear modulus, multiply vertical scale by 10^6).

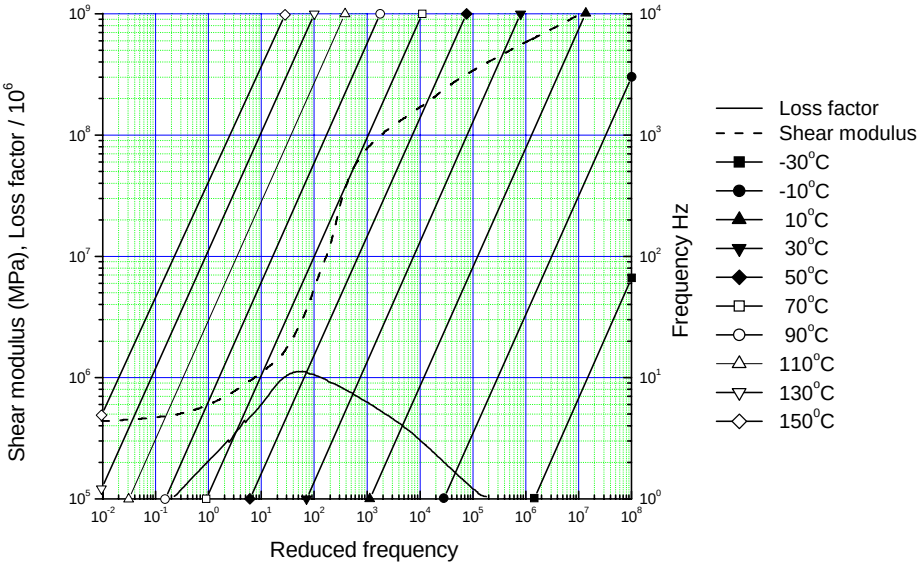

Figure 8: Dyad 609 material data. (To obtain loss factor divide shear modulus scale by 10^6)

The proposed design of the highly damped repair is the configuration shown diagrammatically in Figure 6. The theory developed here is applicable to simply supported or fully clamped rectangular plates. However, for best results the edge support conditions should allow for shear deformation of the viscoelastic damping layer, as shown in Figure 6, otherwise the maximum possible loss factor will not be achieved. Note that both an erosion layer and sealant were necessary to protect the repair.

For the design of the repair the following points were considered:

a) The constraining layer had an equivalent stiffness to the plate being repaired.

b) The damping material was chosen such that optimal damping occurs for operation in the expected temperature range. In this case Soundcoat Dyad 609 was chosen. The values of η_2 and shear modulus $G_2^{'}$ are obtained from Figure 7 or Figure 8 for Dyad 606 and Dyad 609 materials, respectively [14], using the procedure covered in Section 3. Also the thickness of the damping layer must be specified.

c) The load to be applied was the power spectral density (PSD) of the excitation, as described in Section 4.

d) Determine the computation of the stress intensity, stresses, strains and lateral deformation as described in Section 5.

e) Assess the thermal residual stresses as presented in Section 6.

f) Determine crack growth rates as detailed in Section 7.

2.2 Edge support conditions

Experimental evidence indicated that fatigue cracking usually occurred along the edges of the plate rather than in the centre of the plate. This suggests that, as a first approximation, clamped edge conditions are appropriate.

3. Damping materials

Damping data is shown in Figure 7 and Figure 8 for Soundcoat Dyad 606 and 609, [14]. To obtain the damping properties from these plots follow the steps, below with reference to Figure 9:

(a) For the specific panel resonant frequency (right hand scale) project horizontally to intersect the appropriate oblique temperature curve.

(b) Now intersect the shear (storage) modulus curve vertically and read off the shear Storage modulus from the left hand scale.

(c) Obtain the loss factor by intersecting the loss factor curve vertically and read off the corresponding loss factor from the left hand scale.

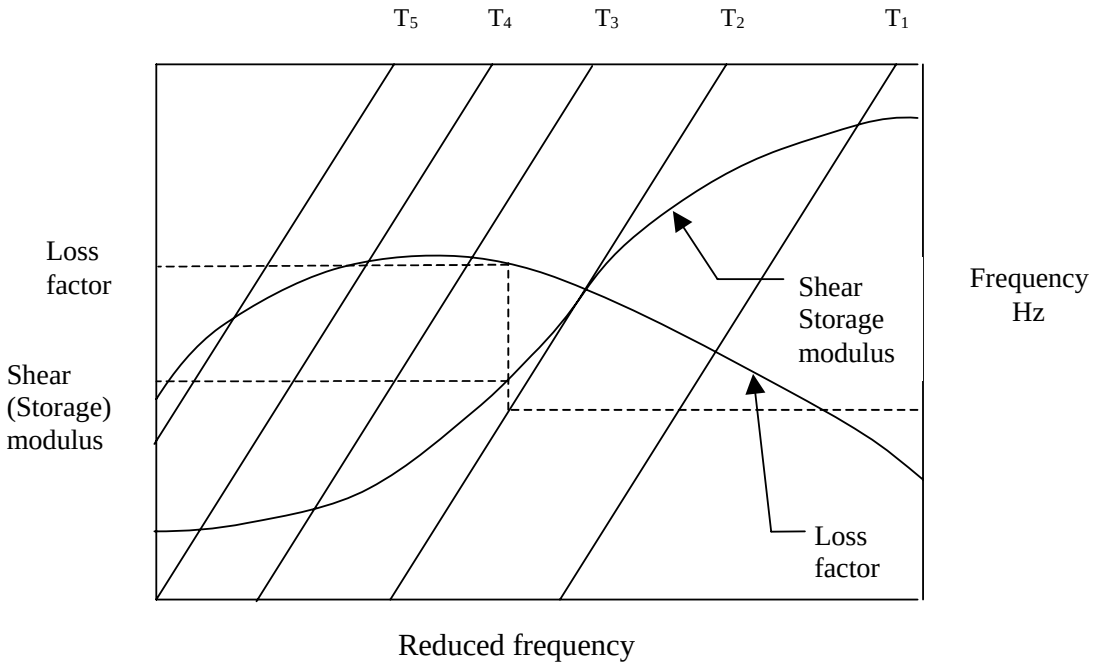

Figure 9: Procedure to determine damping properties at the required frequency and temperature. Higher values of the subscipt i for T_i indicate increasingly higher temperatures

4. Sound pressure levels

Sound pressure levels (SPL) measured on the external surface of an F/A-18 inlet nacelle are plotted in Figure 10. The spectrum level, relative to the overall sound pressure level (OASPL), was derived from in-flight one-third octave SPL measurements, [2]. This spectrum level is now used to calculate the PSD of the excitation, $S_I(f_0)$. OASPL pressure levels of 172.2dB have been measured on the inlet nacelle [2].

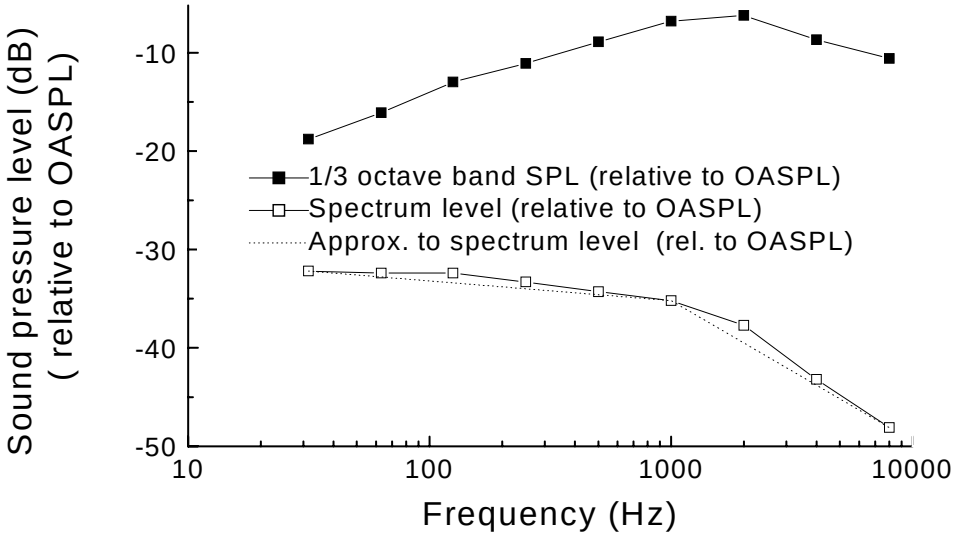

Figure 10: Spectrum and one-third octave band levels of sound pressure over the external nacelle inlet (where OASPL=172.2 dB) [2].

The relationship between the spectrum SPL and the root-mean-square (r.m.s) of the fluctuating pressure p, (Pa), is given by [15] as:

$$p_{rms} = 10^{SPL/20 - 4.65894} \tag{24}$$

and the power spectral density of acoustic pressure, i.e. PSD of the excitation, at any given frequency is given by:

$$S_I(f_o) = p_{rms}^2 = 10^{SPL/10 - 9.3979} \tag{25}$$

The curve in Figure 10 has been approximated by two straight lines defined by the three points listed in Table 2 and is also shown in Figure 10. This approximate spectrum is used as the excitation PSD for the finite element analysis.

Table 2: Input power spectral density corresponding to an OASPL of 172.2 dB

Frequency (Hz)	Three points to approximate curve (dB)	Pressure spectrum level (dB)	$S_I(f_0)$ (MPa)^2 / Hz
31.5	-32.2	172.2 - 32.2 = 140	4.0×10^{-8}
1000.	-35.2	172.2 - 35.2 = 137	2.005×10^{-8}
8000.	-48.1	172.2 - 48.1 = 124.1	1.028×10^{-9}

From Table 2, it is possible to change the spectrum level SPL to any OASPL required. Validation studies outlined in Appendix A show that a good match between experimental data and predicted strains occurs at an OASPL of 159 dB.

5. Computation of stress intensity factor

Acoustic fatigue is associated with the random loading of a structure over a wide frequency range. In the case considered here, the loading is applied to a rectangular panel shown in Figure 4. The complete analytical solution of the dynamic response of the panel is very complex [19]. However, in the case of acoustic fatigue, a number of assumptions can be made, as the emphasis here is to determine the crack growth driving force. Firstly, the time varying pressure can be considered to be uniform and in phase over the panel. Secondly, since the first mode contributes to 98% of the panel response [3], the contribution of all other modes will be ignored. Also the variation of power spectral density (PSD) may be assumed to be constant with frequency near the first mode frequency. Furthermore, it is assumed that the loss factor using equations (11-13) are applicable to a rectangular plate supported on all sides. The solution [11] is directly applicable to simply supported edges, however a modification may be made to apply to clamped edges. Together with the assumptions of [20], the Miles solution gives the root-mean-square (in time space) of the stress intensity response as:

$$K^{rms} = \sqrt{\frac{\pi f_0 S_I(f_0)}{2\eta_s}}\bar{K} \tag{26}$$

where

K^{rms} is the rms stress intensity factor due to the acoustic loading,

$\bar{K}$ is the static stress intensity factor due to the application of a unit pressure on a structure,

$S_I(f_0)$ is the PSD of the excitation at f_0 (Pa^2/Hz),

f_0 is the first resonant frequency (H_z) which depends on boundary conditions and

η_s is the loss factor.

In general, aircraft skin panels are usually connected to other plates or stiffeners at their boundaries, consequently the acoustic response lies somewhere between the limiting cases of simply supported edges or fully-fixed edges. Cracking on the edge of the longest side suggests that clamped boundary conditions dominate.

5.1 Un-repaired plate

5.1.1 Mode shape

It is necessary to define a mode shape that satisfies the boundary conditions at the edge and centre of the plate. For clamped edge conditions a mode shape has been found from [22] to give good results. This mode shape can be represented by:

$$w(x,y) = w_0 \left[1-4\left(\frac{x}{L_x}\right)^2\right]^2 \left[1-4\left(\frac{y}{L_y}\right)^2\right]^2 \tag{27}$$

where w_0 is the maximum out of plane displacement at the centre of the plate. According to Miles solution, the maximum transverse displacement w_0 at the centre of a plate is,

$$w_0 = \sqrt{\frac{\pi f_0 S_I(f_0)}{2\eta_s}}\ W(L_y/L_x)\frac{L_x^4}{E_1 h_1^3}, \tag{28}$$

where $W(L_y/L_x)$ is given in ref [24]; the numerical values for a clamped panel can be approximated by ref [35]

$$W = 0.0284e^{-0.754(L_x/L_y)^{3.79}}, \tag{29}$$

Hence the displacement at any point is given by,

$$w(x,y) = \sqrt{\frac{\pi f_0 S_I(f_0)}{2\eta_s}}\ W(\frac{L_y}{L_x})\frac{L_x^4}{E_1 h_1^3}\left[1-4\left(\frac{x}{L_x}\right)^2\right]^2\left[1-4\left(\frac{y}{L_y}\right)^2\right]^2. \tag{30}$$

Computational validation is described in Table A1 of Appendix A.

5.1.2 Resonant frequency

For the case of an un-repaired plate with all edges clamped, it is assumed that the crack is small enough that it does not significantly affect the first resonant frequency. Hence the first mode frequency is given by:

$$f_0 = \frac{1}{2\pi}F(L_y/L_x)\sqrt{\frac{D_t}{\rho\ h\ L_x^4}} \tag{31}$$

where ρ is the density, L_x and L_y are the length and width of the plate respectively. The parameter $D_t = Eh^3/12(1-\nu^2)$ denotes the bending stiffness. The geometry factor $F(L_y/L_x)$ is given in ref [24]. For the case of clamped edges, the geometry factor can be approximated by ref [35],

$$F = e^{0.477(L_x/L_y)^{2.3}}, \tag{32}$$

5.1.3 Strain and stress

The deformation of an un-repaired plate under acoustic loading is of pure bending, with the bending strain along the x-direction being given by,

$$\varepsilon_b = \frac{h_1}{2}\frac{\partial^2 w}{\partial x^2}. \tag{33}$$

Along the clamped edge y=0, the root-mean-square of the bending strain becomes

$$\varepsilon_b^{rms} = \sqrt{\frac{\pi f_0 S_I(f_0)}{2\eta_s}}\, W(\frac{L_y}{L_x})\frac{L_x^4}{E_1 h_1^3}\frac{h_1}{2}\frac{16}{L_x^2}\left[12\left(\frac{x}{L_x}\right)^2 - 1\right] \tag{34}$$

With the strain parallel to the clamped edge being zero, the rms value of the bending stress is

$$\sigma_b^{rms} = \frac{E_1}{\left(1-\nu_1^2\right)}\sqrt{\frac{\pi f_0 S_I(f_0)}{2\eta_s}} W(\frac{L_y}{L_x})\frac{L_x^4}{E_1 h_1^3}\frac{h_1}{2}\frac{16}{L_x^2}\left[12\left(\frac{x}{L_x}\right)^2 - 1\right] \tag{35}$$

5.1.4 Stress intensity factor

The analysis to determine the stress intensity factor for the plate alone subjected to uniform pressure is given in ref [17]. This analysis is applicable to both simply supported and clamped plates. The bending stress intensity factor of a crack of total length 2*a* is given by,

$$K_b = \sigma_b\sqrt{\pi a\frac{1+\nu}{3+\nu}} \tag{36}$$

Applying the Miles solution, the rms value of the bending stress intensity factor becomes,

$$K_b^{rms} = \sigma_b^{rms}\sqrt{\pi a\frac{1+\nu}{3+\nu}}. \tag{37}$$

with σ_b^{rms} being given by equation (33). Computational validation is described in Appendix A.

5.2 Repaired plate

5.2.1 Mode shape and resonant frequency

The same mode shape for the un-repaired plate is used. For the case of an un-repaired plate with all edges clamped, it is assumed that the crack is small enough that it does not significantly affect the first resonant frequency. When the stiffness of the viscoelastic layer is negligible, i.e., zero, the first mode frequency is,

$$f = \frac{1}{2\pi}F(L_y/L_x)\sqrt{\frac{D_t}{m_t L_x^4}} \tag{38}$$

where $m_t = \rho_1 h_1 + \rho_2 h_2 + \rho_3 h_3$ is the total mass per unit length, and the bending stiffness

$$D_t = \frac{E_1 h_1^3}{12(1-\nu_1^2)} + \frac{E_3 h_3^3}{12(1-\nu_3^2)} \tag{39}$$

and $F(L_y/L_y)$ is given by expression (32) for clamped plate.

The correct frequency for a non-zero or finite stiffness core can be determined by the use of a non-dimensional frequency ratio,

$$\Omega = \sqrt{1 + Y \frac{g_m\left(1 + g_m(1 + \eta_S^2)\right)}{1 + 2g_m + g_m^2(1 + \eta_S^2)}} \quad . \tag{40}$$

The resonant frequency for finite-stiffness core is thus

$$f_0 = \frac{1}{2\pi} F(L_y / L_x)\sqrt{\frac{D_t}{m_t L_x^4}}\Omega \tag{41}$$

Results in Table A1, Appendix A1, show good agreement between solution (27) and the FE analysis.

5.2.2 Strains and stresses in a repaired plate

Following the above derivations, the root-mean-square (RMS) out-of-plane displacement w_0 at the centre of a repaired plate is given by

$$w_0^{rms} = \sqrt{\frac{\pi f_0 S_I(f_0)}{2\eta_s}} W(\frac{L_y}{L_x}) \frac{L_x^4}{E_1 h_1^3 + E_3 h_3^2} \frac{1}{\Omega^2} \tag{42}$$

Using the same mode shape given by equation (27), RMS of the out-of-plane displacement $w(x, y)$ can be expressed as,

$$w^{rms}(x, y) = w_0^{rms} f_1(x) f_2(y) = w_0^{rms}\left[1 - 4\left(\frac{x}{L_x}\right)^2\right]^2\left[1 - 4\left(\frac{y}{L_y}\right)^2\right]^2 \tag{43}$$

The bending strain along y=0 can be derived in a similar way as for the un-repaired plate,

$$\varepsilon_b^{rms} = -\frac{\partial^2 w^{rms}}{\partial x^2}\frac{h_1}{2}. \tag{44}$$

The r.m.s membrane strain in the plate is obtained as (Mead and Markus, 1969)

$$\varepsilon_m^{rms} = \frac{\partial u_1^{rms}}{\partial x} \equiv -\frac{1}{gdE_1 h_1}\left[m_t \omega_0^2 w^{rms} - D_t \frac{\partial^4 w^{rms}}{\partial x^4} + gD_t Y \frac{\partial^2 w^{rms}}{\partial x^2}\right]. \tag{45}$$

Since the strain parallel to the clamped edge is zero, the RMS stresses are

$$\sigma_m^{rms} = \frac{E_1 \varepsilon_m^{rms}}{1 - \nu_1^2}, \tag{46a}$$

$$\sigma_b^{rms} = \frac{E_1 \varepsilon_b^{rms}}{1 - \nu_1^2}. \tag{46b}$$

Using strains, this expression is validated against F.E., and the results are given in Table A1, Appendix A.

5.2.3 Stress intensity factor of repaired plate subjected to acoustic pressure

The most common type of repair applied to aircraft skins are one sided as illustrated in Figure 11, since, in general, access is only available to the outside of the skin. Analytical solutions for one-sided repairs, known as the Wang-Rose model are available for both in-plane [16, 17] and out-of-plane loading [17]. A significant feature of bonded repairs is that the variation of stress

intensity $K(z)$ with crack length does not increase indefinitely with crack length [18, 25]. Instead, the stress intensity approaches an asymptotic value. The thickness of the adhesive is included in the analysis to represent the damping material. The computation of stress intensity was based on the work carried out in ref [11].

Consider the damped plate shown in Figure 11. Depicted in Figure 11a are the components of the damped plate subjected to a lateral loading resulting in a bending moment. In the absence of a crack, the bending stress which varies linearly through the plate thickness is shown in Figure 11a. The Wang-Rose crack bridging theory involves firstly replacing a crack in the damped repair by springs along the face and secondly use of the lap joint analysis to determine the load transfer. This results in the following equations for the membrane stress intensity K_m and the bending stress intensity K_b, assuming the membrane and bending stresses are constant over the crack length,

$$K_m^{rms} = f_{mm}\ \sigma_m^{rms} + f_{mb}\ \sigma_b^{rms} \quad (47a)$$

$$K_b^{rms} = f_{bm}\ \sigma_m^{rms} + f_{bb}\ \sigma_b^{rms} \quad (47b)$$

where f_{mm}, f_{mb}, f_{bm} and f_{bb} are the normalised stress intensity factors. Plots of f_{mm}, f_{bm}, f_{mb}, f_{bb} are shown in Figure 12-Figure 14 for temperatures of -67 °C, 30 °C and 120 °C. Figure 15 shows the variation of the normalised stress intensity factor with temperature. The closed form solutions are in close agreement with FE analysis, as shown in Table A2, Appendix A.

In the present case, as the crack length increases, the prospective membrane and the bending stresses vary along the crack length. In this case, a full crack bridging analysis is required to account for the effect of stress gradient. For an edge crack lying between ($-a$, $L_y/2$) and (a, $L_y/2$), the prospective membrane stress σ_m and the prospective bending stress σ_b both vary with the coordinate. The crack-bridging problem, viz, the integral equations [17], can be solved numerically using a Galerkin method: expand the unknown functions in terms of Chebyshev polynomials and then determine the coefficients numerically. Because the prospective stresses vary with the position along the crack path, the matrix equations become [35]

$$\begin{aligned} \hat{A}_{ij}\hat{f}_j + \hat{B}_{ij}\hat{g}_j &= \frac{1}{E_s}\int_{-1}^{1}\sqrt{1-r^2}U_j(r)\sigma_m(r)dr \quad (i,\ j=0,\ 1,\ 2,\cdots N) \\ \hat{C}_{ij}\hat{f}_j + \hat{D}_{ij}\hat{g}_j &= \frac{1}{E_s}\int_{-1}^{1}\sqrt{1-r^2}U_j(r)\sigma_b(r)dr \quad (i,\ j=0,\ 1,\ 2,\cdots N) \end{aligned}, \quad (48)$$

where U_j denotes the Chebyshev polynomials of the second kind.

Figure 16 shows the frequency function for the variation of the first mode of a rectangular plate for all edges simply supported or all edges clamped.

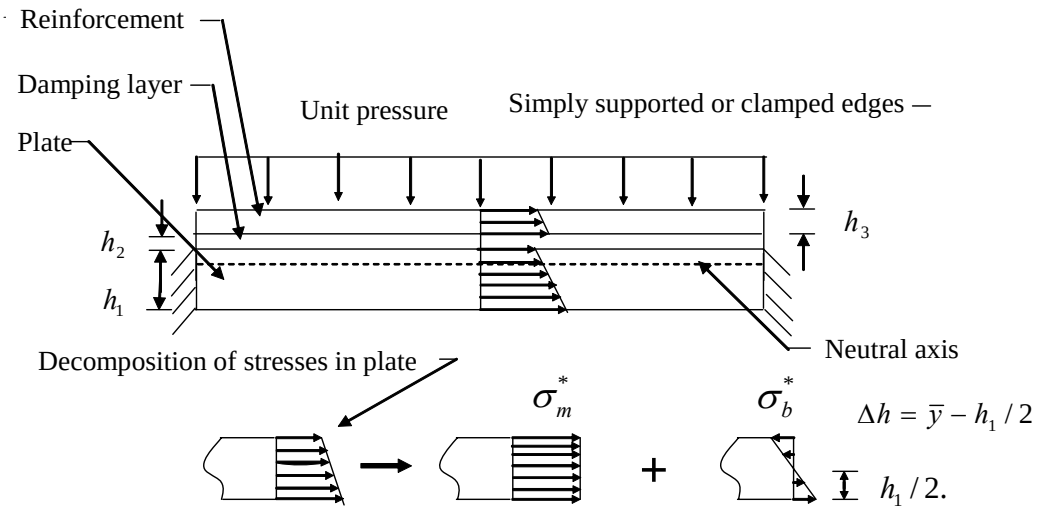

(a) 2D view of un-cracked reinforced case

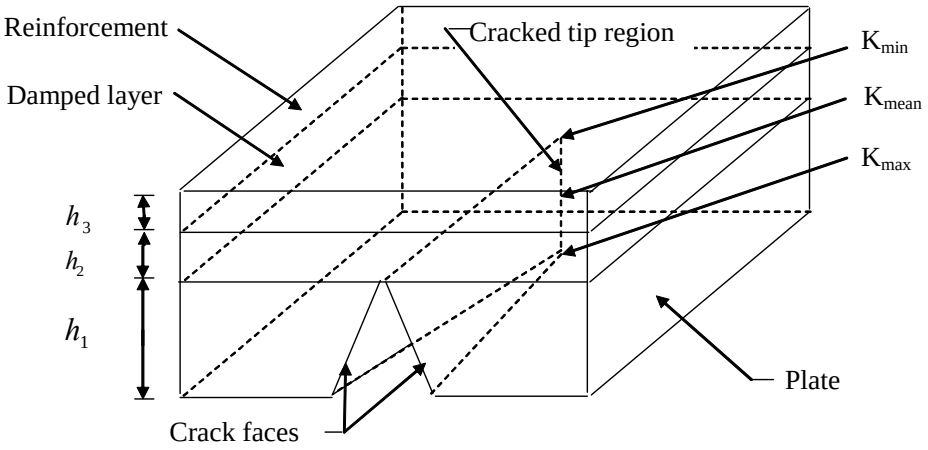

(b) 3D section view: cracked and repaired case

Figure 11: One sided repair consisting of a reinforced beam subject to one unit of lateral pressure

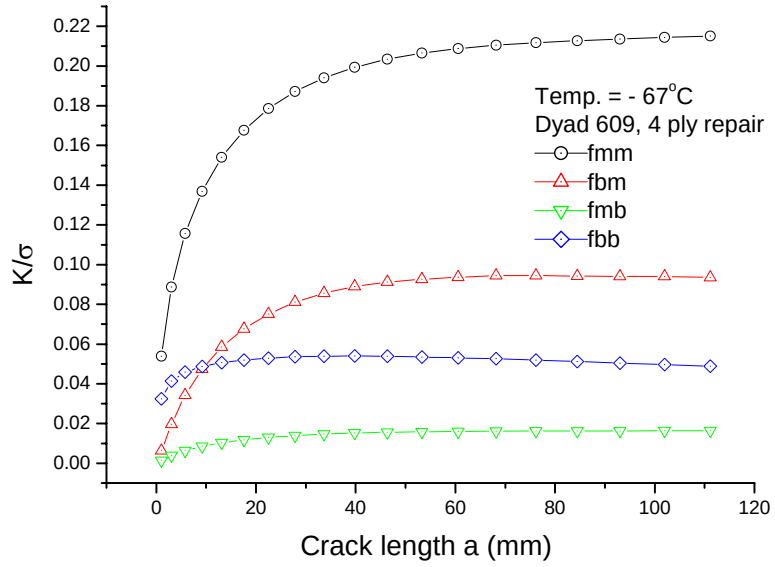

Figure 12: Results from Wang-Rose crack bridging model [17] for lateral static loading at -67 °C

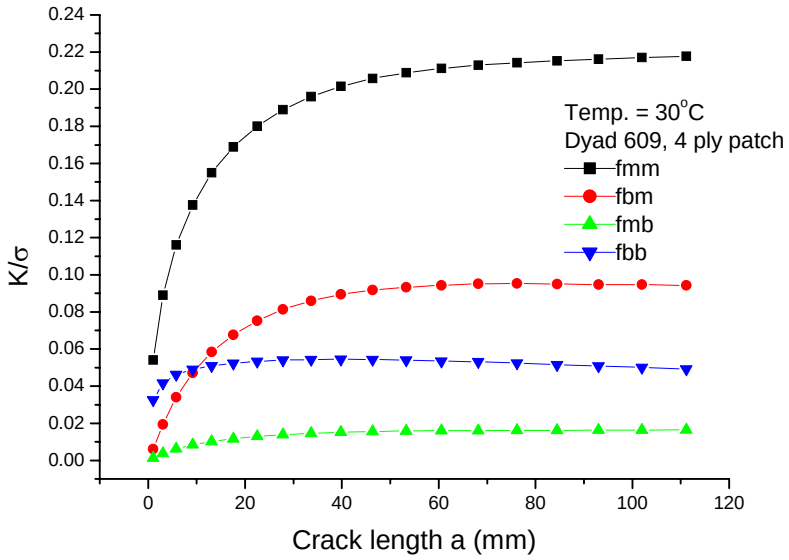

Figure 13: Results from the Wang-Rose crack bridging model [17] for lateral static loading at 30 °C

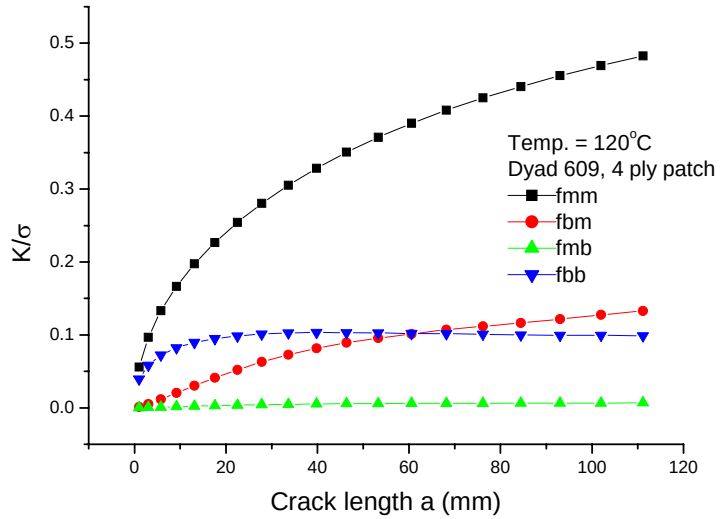

Figure 14: Results from the Wang-Rose crack bridging model [17] for lateral static loading at 120 °C

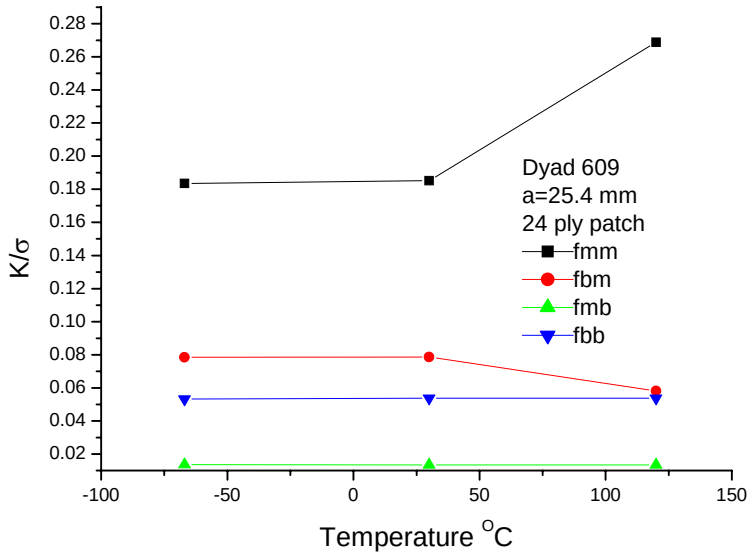

Figure 15: Results from the Wang-Rose crack bridging model [17] for lateral static loading and crack-length a= 25.4 mm

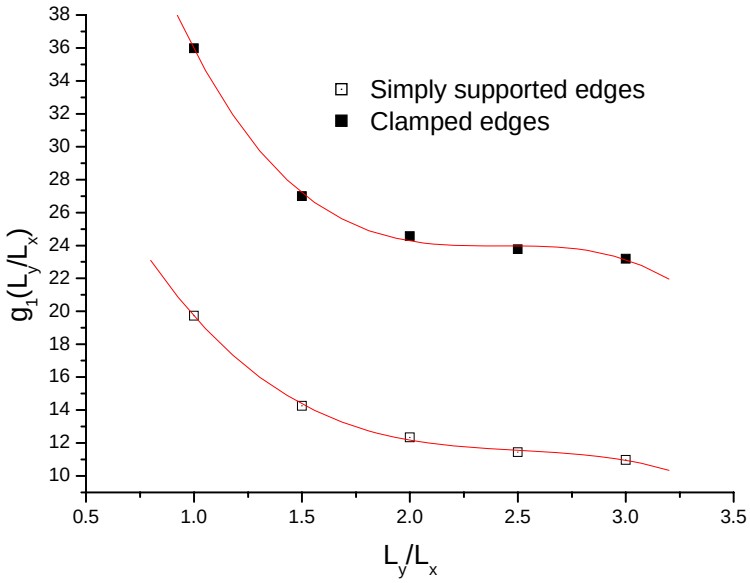

Figure 16: Frequency function for first mode of a rectangular plate, all edges clamped and all edges simply supported.

6. Residual thermal stresses

At a given operating temperature, the thermal stresses can be considered as the superposition of the thermal stresses due to two steps: the curing of the adhesive (involving a localized heating-cooling cycle) and a uniform temperature change from the room temperature to the operating temperature. For an aircraft panel that is riveted on to stiff frames, the aircraft skin is completely restrained from expansion and contraction during the heating-cooling cycle. Consequently no thermal stress will develop as a result of the bonding of the repair patch.

During operations the aircraft skin temperature can drop to as low as -67 °C. With the aircraft skin being stiffened by the repair and constrained by frames, a high thermal stress will occur in the repair and the skin. A conservative approach is to assume that all edges of the skin panel are completed constrained, i.e., the total strain remains zero. The resulting thermal stresses in the skin are given by,

$$\sigma_{xx}^{T} = \sigma_{yy}^{T} \equiv \frac{1}{1-\nu}\alpha_1 E_1 (RT - T_{oper}) \tag{49}$$

where RT and T_{oper} denote respectively the room temperature and the operating temperature, also the thermal coefficient of expansion of the plate is denoted by α_1. The above expression furnishes an upper-bound estimate of the thermal stresses.

A lower-bound estimate of the thermal stresses can be obtained by assuming that the frames experience the same temperature change as the skins. In this case, the problem can be viewed

as a large plate containing a small patch. The thermal stress in the skin, underneath the patch, is given by the Rose and Wang [34],

$$\sigma_{xx}^{T} = \sigma_{yy}^{T} \equiv \frac{(1+\nu_1)(1-\alpha_3/\alpha_1)S}{2(1-\nu_3)+(1-\nu_1^2)S}\alpha_1 E_1 (RT - T_{oper}) \tag{50}$$

where S denotes the stiffness ratio given by,

$$S = E_3 h_3 / E_1 h_1 \tag{51}$$

The above thermal stresses are membrane stresses. The stress intensity factor associated with the thermal stresses are

$$K_m^T = \sigma_{xx}^T f_{mm} \tag{52}$$

$$K_b^T = \sigma_{xx}^T f_{bm} \tag{53}$$

$$K_T = K_m^T + K_b^T \tag{54}$$

The influence of thermal stresses on fatigue crack growth rates will be discussed in the following section.

7. Crack growth model

By comparing data from standard crack growth laws [28] with acoustic data [27] it has been found that good agreement exists. The standard crack growth laws are intended to be accurate from 6 to 50 $\mathrm{MPa}\sqrt{\mathrm{m}}$, and apply to in-plane tension cycling only. The threshold stress intensity factor for crack growth under high frequency out-of-plane bending may be higher [29] than for in-plane loading. The crack growth law for 7075-T6 is given by [29] as:

$$\frac{da}{dn} = C_f (\Delta K)^m \left[1 - \left(\frac{\Delta K_{th}}{\Delta K}\right)^2\right] \text{(mm/cycle)} \tag{55}$$

where $C_f = 2.1\times10^{-7}$, $m = 3.02$. Here ΔK is assumed to be equal to ΔK_{rms}, and ΔK_{th} is the threshold stress intensity factor for crack growth.

7.1 Crack growth threshold

Data derived from [29] indicates that the crack growth threshold for peak values of stress intensity, ΔK_{th}, factor is approximately $10\ MPa\sqrt{m}$.

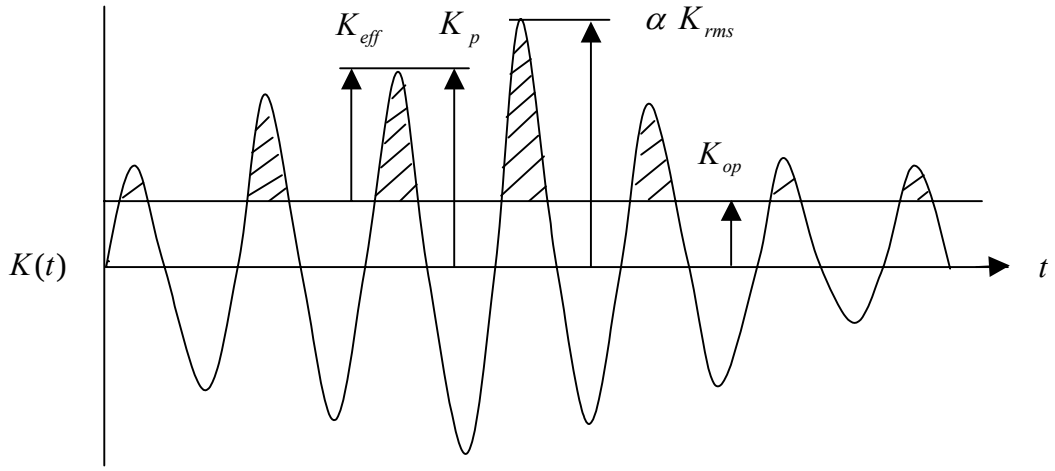

Figure 17: Effect of crack closure in random bending, variation of K with time [30]

7.2 Crack closure

It is known that under cyclic lateral loading, plasticity will occur at the crack tip [30]. As a result, during the second tension cycle there will be a delay until the crack opens. The fraction of the load at which the crack opens is defined as β. As shown in Figure 17, the time history for a random event in which a maximum peak occurs is defined by αK_{rms}. From [30] the effective (peak) stress intensity factor due to crack closure is given by:

$$\Delta K_{eff} = K_p - \alpha \beta K_{rms} \quad (56)$$

Using the values of α and β available from [30], i.e., α=3.75 and β=0.3 respectively, the effective K is

$$\Delta K_{eff} = K_p - 1.125 K_{rms} \quad (57)$$

7.3 Crack growth for narrow random crack growth

It is also known that during cyclic lateral bending crack closure of the plate may occur when the surface of the plate is in tension. This results from the plastic zone at the tip of the growing crack. Since this plastic zone will remain in the wake of the crack, unloading of the crack will result in crack closure before complete unloading occurs. From [30] a peak probability distribution has been used as representative of acoustic loading and exhibits a “truncated” probability distribution in which peaks above a certain level do not occur. From flight trials data [31] the ratio of peak values to rms values is 5.

7.3.1 Case A

If the stress intensity factor at which the crack opens ($\alpha\beta K_{rms}$) is greater than the peak value of the threshold stress intensity $\sqrt{2}\ K^t_{rms}$ then peaks less than $\alpha\beta K_{rms}$ will not contribute to the crack growth.

i.e. $\alpha\beta K_{rms} \geq \sqrt{2}\ K_{rms}$ (58)

$$\frac{da}{dN} = \frac{C}{(1.-\beta^2)^n} K^n_{rms}\ I(\ n, \frac{\alpha^2\beta^2}{2.}, \frac{\alpha^2}{2.}, \frac{\alpha^2\beta^2}{2.}) \tag{59}$$

7.3.2 Case B

If $\alpha\beta K_{rms}$ is less than $\sqrt{2}\ K^t_{rms}$ then this will not result in crack growth, due to a threshold effect. In this case,

$$\frac{da}{dN} = \frac{C}{(1-\beta^2)^n} K^n_{rms}\ \ I\ (\ n, \frac{\alpha^2\beta^2}{2.}, \frac{\alpha^2}{2.}, \frac{(K^t_{rms})^2}{K^2_{rms}}) \tag{60}$$

where

$$I\ (n, d, h, l\ ) = \int_l^h (\ t^{1/2} - d^{1/2})^n\ e^{-t}\ dt\ . \tag{61}$$

The alternative to solving these equations is to design the repair such that $K \leq 10\ K_p$, for 7075-T6.

8. Acoustic loading on F/A-18

While data exist [2] for the SPL on the inlet nacelle region, there is no data for the aft fuselage region. It was reported that the airframe [2] was designed for an overall sound pressure level (OASPL) of 160 dB. Flight trials [31] in which a dosimeter was installed to measure the strains on two adjacent skin panels with and without repair, respectively, have provided both peak and r.m.s. strain data on the aft fuselage region. For the un-repaired panel two strain gauges were used, with one gauge at the centre of the panel and the other at the edge of the panel. Since the centre gauge was in a region of low strain gradient, the measured strains are more reliable than the gauge close to the edge. Assuming that the mode shape is the fundamental mode, it is possible to back-calculate the OASPL from the centre strain gauge data. These calculations are described in Appendix A and show that the OASPL in the region of the aft fuselage is 159 dB, very close to the design level of 160 dB.

9. Highly Damped Repair, Example

An example problem such as a highly damped repair for the aft fuselage of the F / A-18 will be considered. Data needed for this design are shown in Table 3, Table 4 and Table 5. The various parameters used in the analysis are shown in Table 7. The expected operating temperature of the F / A-18 in the vicinity of the aft fuselage is -67 to +120 °C.

Table 3: Details of parameters for the highly damped repair example

Item	Value	Description
ΔT	40 °C *	From curing temperature to operating temperature.
α_1	23.x10^{-6} /°C	Thermal coefficient of expansion of plate.
α_3	5.57x10^{-6} /°C	Thermal coefficient of expansion of constraining layer.
h_1	0.9 mm	Thickness of plate.
h_2	0.508 mm	Thickness of damping layer.
h_3	0.508 mm	Thickness of constraining layer.
E_1	71000 MPa	Young's modulus plate.
E_3	113300 MPa	Modulus of constraining layer.
ν_1	0.3	Poisson's ratio for plate.
ν_3	0.0535	Poisson's ratio for constraining layer.
ρ_1	2.77x10^{-9} kkg / mm^3	Density of plate.
ρ_3	2.03x10^{-9} kkg / mm^3	Density of constraining layer.
ρ_2	1.10x10^{-9} kkg / mm^3	Density of viscoelastic material.
L_x	175 mm	Length of plate.
L_y	176 mm	Width of plate.
$[K_O / \sigma]$		Coefficients from Figures 12-15, depending on crack size.
m	3.02	Parameter for crack growth law for 7075-T6.
C_f	1.37x10^{-5}	Parameter for crack growth law for 7075-T6.
K_f	63.9	Parameter for crack growth law for 7075-T6.
η_2	1.0 *	Loss factor for viscoelastic damping layer.
η_1	0.013	Loss factor for plate.
η_3	0.004	Loss factor for composite.
G_2	10 MPa *	Shear modulus for damping layer.

* variables for example problem

Table 4: Loss factor and shear modulus for Dyad 606 versus operating temperature corresponding to cure temperature of 90 °C, from Figure 7

Operating temp. °C	Temperature Change °C	Loss factor $\eta + \eta_t$	G_2 (MPa)
-67	157	0.01912	300
-40	130	0.01912	300
-20	110	0.01912	300
0	90	0.01912	300
20	70	0.02025	300
30	60	0.1749	70
40	50	0.4171	17
50	40	0.3619	5
60	30	0.1385	2
70	20	0.04151	0.7
80.	10	0.02391	0.4
90	0	0.02146	0.4

Table 5: Loss factor and shear modulus for Dyad 609 versus operating temperature corresponding to cure temperature of 90 °C, from Figure 8

Operating temp. °C	Temperature Change °C	Loss factor $\eta + \eta_t$	G_2 (MPa)
-40	130	0.02109	300
-20	110	0.02109	300
0	90	0.02109	300
20	70	0.03224	300
30	60	0.04088	280
40	50	0.05717	200
50	40	0.09915	130
60	30	0.14563	85
70	20	0.23625	50
80.	10	0.36454	25
90	0	0.40449	5

Table 6: PSD of the excitation for plate alone, also the repaired case, interpolated from Figure 10 from results for inlet nacelle[2]

OASPL (dB)	S_I (197 Hz)	S_I (344 Hz)
159	2.196×10^{-9}	2.015×10^{-9}

Table 7: Terminologies used in Mathematica program

Quantity	Equation/comment
s	47, Stiffness ratio
Ω	37, Frequency correction for non-zero core
f_0	29, Natural frequency for plate
f_c	35 Natural frequency for repaired plate
PSD	24, Power spectral density
g_m	18, Geometric shear factor
k_f^2	19, Wave number
Y	3, Geometric factor
η_t	12, Loss factor due to skin and patch
η_c	Loss factor for viscoelastic material see Figures 7 or 8.
η_S	10, Loss factor due to η_1, η_2, η_3
$\eta_{DC,m}$	15, overall loss factor
g_{opt}	22, Can be ignored, this is only needed for optimum design
$\eta_{s\max}$	21, Can be ignored, this is only needed for optimum design
w_0	28, 42 transverse displacement
ε_m^{rms}	43, Membrane strain in patched plate
ε_b^{rms}	42, Bending strain in patched plate
σ_m^{rms}	45a, Membrane stress in patched plate
σ_b^{rms}	45b, Bending stress in patched plate
K_m^{rms}	46a Membrane stress intensity factor for repaired panel
K_b^{rms}	46b Bending stress intensity factor for repaired panel
ΔK_p	69, Delta, peak stress intensity factor (ratio peak / rms is 5)

The analyses described in Section 5 have been implemented using a symbolic solver Mathematica. Consider a plate of dimensions $L_x = 176, L_y = 175$ mm and thickness $h_1 = 0.9$ mm with a repair of $L_x = 176, L_y = 175$ mm and thickness $h_3 = 0.508$ mm, which corresponds to four layers of boron for the constraining layer as shown in Figure 4. The aim is to achieve a neutral axis within the viscoelastic material in order to maximise the shear, although distances away from the neutral axis are not far from the optimum. Consider an operating temperature of –40 to 90 °C. In this case, Dyad 609 is used due to durability concerns of Dyad 606 at high temperature. Dyad 609 material only comes in at thicknesses of 0.508 and 1.106 mm. A thickness of 0.508 will be used. For the boron doubler, a stacking sequence of [0 / 90 / 0 / 90] will be used, resulting in a laminate modulus of 114 GPa.

Firstly, from experimental data [29], both the loss factor and the resonant frequency change with increasing moisture content. Note that the un-conditioned specimen gives higher loss factors than data provided by the manufacturer. The difference is due to moisture uptake

whereas the manufacturer's data is for low humidity. A change of resonant frequency indicated that the shear modulus also changed with moisture. These are factors that may have to be considered in determining the real loss factor. For this exercise the manufacturers data will be used, see Figure 18.

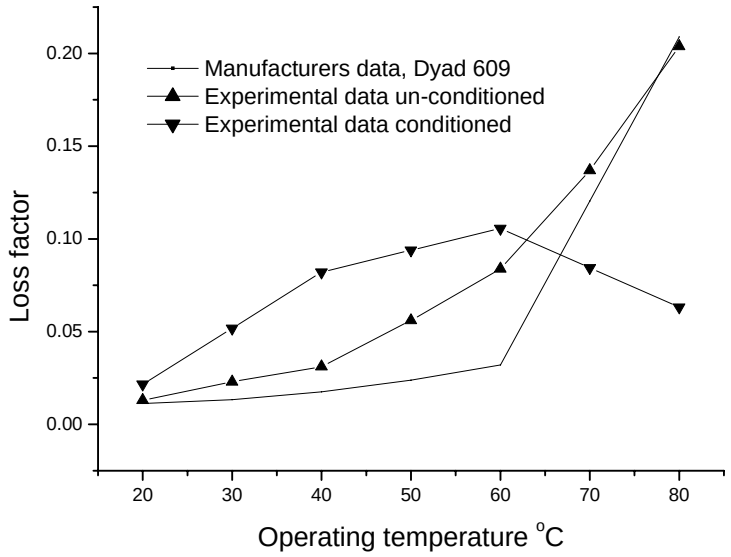

Figure 18: Loss factor versus operating temperature at OASPL=159 dB, for manufacturers data, and conditioned data, this corresponds to a 4 ply configuration

The equations, with parameters given in Table 7, can be solved numerically or symbolically using Mathematica™. The stress intensity factors can then be computed for a range of operating temperatures and SPL's. The corresponding PSD of the excitation is tabulated in Table 6 for a plate with and without repair. The material properties of Dyad 606 and 609 are listed in Table 4 and Table 5 respectively, for various operating temperatures. These results are graphically displayed in Figure 19 and Figure 20 for OASPL of 159 dB and operating temperatures from –67 to 120 °C. In Figure 20 the peak microstrain for Dyad 606 and 609 is 2000 and 955 respectively. Note that the strain level of 1750 microstrain corresponds to the un-patched panel derived from flight trials results. Cleary the Dyad 609 patch has reduced the strain by a factor of almost 2. Note that the Dyad 606 design increases the maximum strain at high temperatures to a level exceeding the flight trial strains on the un-patched panel. This is the result of the damping material having a very low shear modulus at higher temperatures, with the additional mass of the damped layer increasing resonant response. Also shown in Figure 19 is the threshold value for crack growth. As discussed Section 7.1, the threshold value of 10 MPa $m^{0.5}$ was determined from an experimental study, ref [29]. It is evident that from Figure 21 that the 4 ply Dyad 606 design will not survive the high temperature loading. Also the Dyad 609, 4 ply design, is just above the threshold at low temperatures. However, it is expected that when using Dyad 609 a six-ply design will suffice, see Section 9.6

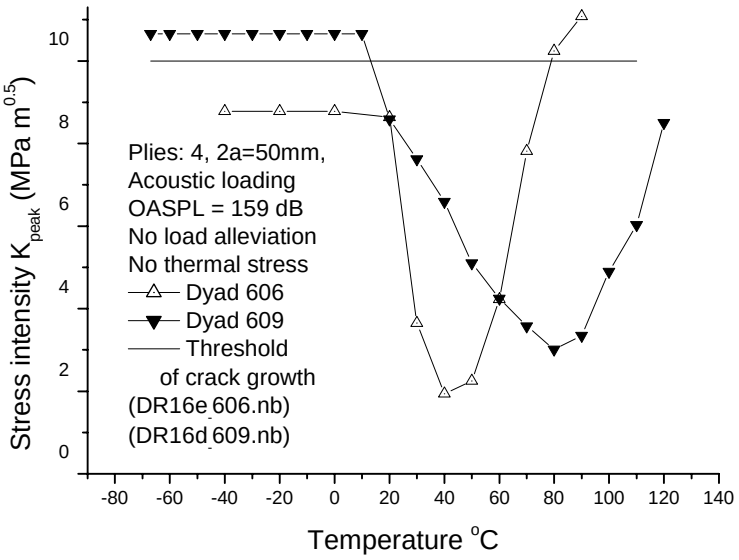

Figure 19: Predicted rms stress intensity factor versus operating temperature at OASPL=159 dB, using Dyad 609 or 606, for crack length 2a=50 mm, this corresponds to a 4 ply configuration where thermal stresses due to uniform temperature change have been ignored.

9.1 Adhesives for the repair

Further considerations concerning the real operating temperatures were made in [33]. For the coldest day the entire aircraft skin temperature is -67 °C. For the hottest day of the year the repair was adjacent to both 103 °C and 141°C temperature regions. As a result an average hottest day was taken to be 122 °C, and the analysis was carried out at 120 °C. The adhesive used to construct the patch was FM300, which was co-cured with the boron and damping material at 177 °C. The adhesive used to bond the repair to the aircraft skin was FM300-2 since this adhesive would perform within the range of -67 °C to 120 °C. Figure 24 and Figure 25 show schematically the structural components of the patch system, and the thickness of each component. In this section adhesive shear stresses due to an acoustic loading will be evaluated.

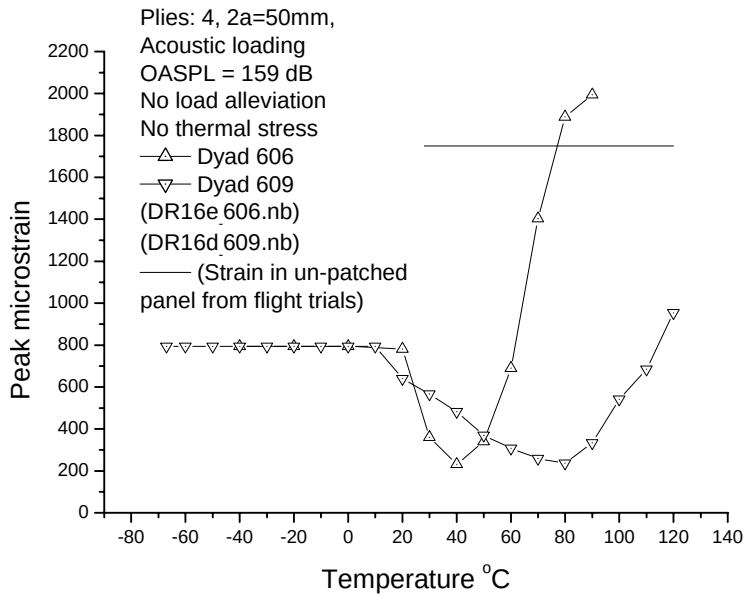

Figure 20: Predicted peak microstrain for repaired panel versus operating temperature for OASPL=159dB, using either Dyad 609 or Dyad 606. This corresponds to 4 ply configuration.

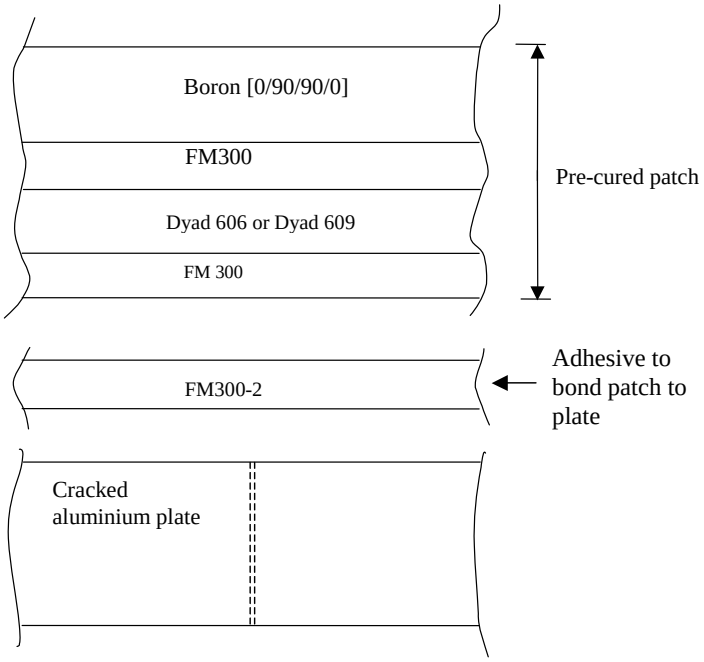

Figure 21: Through thickness view of the individual structural components for the repair of the plate

The dimensions and material properties are shown in Figure 8 and Figure 9.

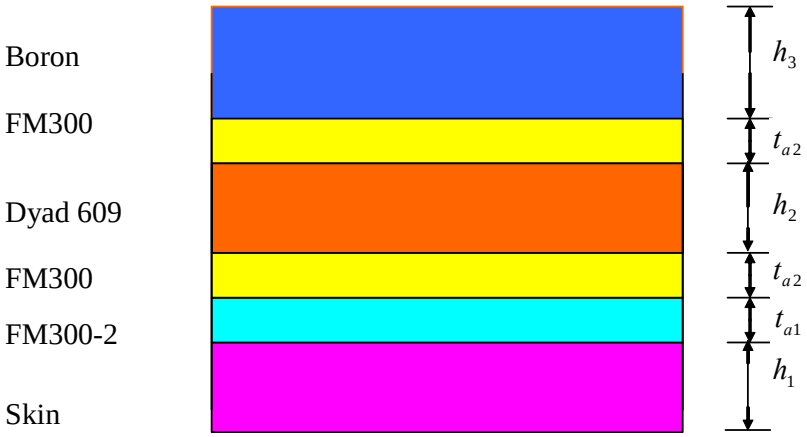

Figure 22: Diagram showing thicknesses of patch components

Table 8: Parameters for adhesive shear stress

Temp. °C	G_{a1} (MPa) FM300-2	G_{a2} (MPa) FM300	G_2 (MPa)	t_{a1} (mm)	t_{a2} (mm)	h_2 (mm)
120	199	199	1	0.127	0.127	0.508
0	415	4150	300	0.127	0.127	0.508

Table 9: Adhesives shear stress due to acoustic loading, using parameters from Table 8

E_1 (MPa)	E_3 (MPa)	h_1 (mm)	h_3 (mm)	σ_m (MPa)	σ_b (MPa)	τ_P* (MPa)	** $\tau_{p\ peak}$ (MPa)
71000	114000	0.9	0.762	0.544	14.662	14.	0.304
71000	114000	0.9	0.762	6.621	6.036	43.	3.540

* is the plastic value of the shear stress for the adhesive

** is the peak value, $\tau_{peak} = 5.*\tau$ (Mathematica :*Damped Repair 16e_609b.nb*)

The shear stress in the adhesive due to acoustic loading, which induces membrane and bending stresses (σ_m and σ_b), is given by,

$$\tau = \frac{G_a^* l}{t_a^*}\left[\frac{\sigma_m + \sigma_b}{E_1}\right], \tag{62}$$

where

$$\frac{t_a^*}{G_a^*} = \left(\frac{t_{a1}}{G_{a1}} + 2\frac{t_{a2}}{G_{a2}} + \frac{h_2}{G_2}\right), \tag{63}$$

$$l = \left[\left(\frac{t_{a1}}{G_{a1}} + \frac{2t_{a2}}{G_{a2}} + \frac{h_2}{G_2}\right)\frac{E_1 E_3 h_1 h_3}{(E_1 h_1 + E_3 h_3)}\right]^{1/2} . \tag{64}$$

The parameters G_{a1}, G_{a2} and G_2 denote the adhesive shear moduli for FM300-2, FM300, and the damping layer respectively. The Young's moduli of the skin and the patch are denoted respectively as E_1 and E_3. Parameters h_1, h_2 and h_3 denote the thickness of the skin, the damping layer, and the patch respectively. The thickness of the FM300-2 and FM300 adhesives are t_{a1} and t_{a2}. Parameters α_{Alum} and α_{Boron} denote the coefficients of thermal expansion for the skin and patch respectively.

For acoustic loading the shear modulus of the adhesive varies with temperature, see Figure 23 for the stress strain curve.

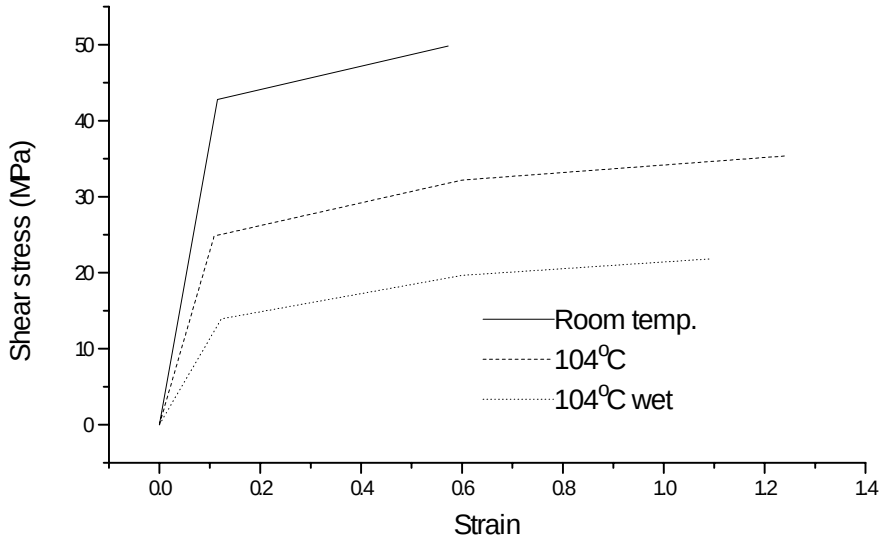

Figure 23: Stress strain diagram for FM300 for the temperature range shown

Calculations in Table 8 and Table 9 for acoustic shear stresses in the adhesive have shown that at an operating temperature of 0 or 120 °C, both FM300 and FM300-2 are operating within the elastic region, hence no fatigue damage will occur, see Table 8 and Table 9. The FM300 is cured in the autoclave at 177 °C, together with the boron and damping material. FM300-2 is used to bond the patch to the aircraft skin at a temperature up to 120 °C.

9.2 Alternating stress intensity factor

The effect of low temperatures may result in tensile residual stresses which would keep the crack open, thus increasing crack growth rates. In this case a simple and conservative approach is to assume that negative stress intensity factor does not contribute to crack growth. In this case, the effective crack growth driving force can be expressed as

$$\Delta K_{eff} = \min(K_{\max}, K_{\max} - K_{\min}) \quad , K_{\max} > 0 \tag{65}$$

Under acoustic loading, the minimum stress intensity factor $K_{\min}$ is equal in magnitude to the maximum stress intensity factor but opposite in sign, *i.e.,* $K_{\min} = -K_{\max}$. In the presence of thermal residual stress intensity factor K_T, the effective range of stress intensity factor is:

$$\Delta K_{eff} = 2K_{\max}, \qquad K_T > K_{\max} \tag{66a}$$

$$\Delta K_{eff} = K_{\max} + K_T, \quad K_T \le K_{\max} \tag{66b}$$

A conservative assumption for the $K_T \le K_{\max}$ case is:

$$\Delta K_{eff} = K_{\max} \tag{67}$$

9.2.1 Small patch

When a small patch is applied, due to the lack of constraint, high residual thermal stress will exist in the skin after the bonding of a Boron patch. As shown in Table 10, the thermal stress intensity factor is approximately equal to the peak stress intensity factor at 20 °C. Therefore, the effective range of the stress intensity is:

$$\Delta K_{eff} = K_{\max} + K_T \approx 2K_{\max} \tag{68}$$

This means that small patches will have large thermal residual stresses and may not prevent crack growth.

9.2.2 Large patch

For a large patch that covers the entire bay (panel) that is riveted to the airframe, no thermal expansion or contraction would occur during the bonding process. As a result, the repaired skin will not experience any thermal residual stress, *i.e.,* $K_T = 0$. For proof see Appendix A.3, in this case:

$$\Delta K_p = K_{\max} \tag{69}$$

It is clear that the effective crack growth driving force would be much less than that pertinent to a small patch. This is consistent with the previous failed-attempt of repairing the acoustic fatigue crack with a small Boron patch that covered only the cracked region.

9.2.3 Case $K_T \geq K_{\max}$

At low temperatures thermal mismatch may result in a high stress intensity factor for the combination of aluminium and boron. As result during each cycle, $\Delta K_{eff} = 2\, K_{\max}$.

9.2.4 Case $K_T \leq K_{\max}$

In this case at high temperatures the value of K_T may be negative. Since crack closure cannot occur then, $K_T = 0$ and $\Delta K_{eff} = K_{\max}$.

9.3 Repair for case of uniform change of temperature

Consider the case for an aircraft which is not subjected to acoustic loading or flight loads and does not contain a patch. Now consider two points on the structure located far apart at opposite ends of the structure. Uniform heating or cooling of the whole structure will result in a relative increment in displacement between the two points. If these points are brought near each other then the relative displacement will decease. At the limit at which no separation exists, the relative displacement is zero. If a crack is introduced into the structure and each point is located on the opposite crack face then heating or cooling will not result in any relative displacement of the crack faces.

If we now apply a patch which is small in comparison to the complete aircraft structure then the stiffness of the structure will not change. As a result the crack opening displacement will be almost zero. Hence uniform heating or cooling will not affect the crack. The only crack opening will occur from acoustic excitation. Flight loads are small in comparison to high acoustic loading.

9.4 Residual stresses from bonding the patch

Bonded repairs involve heating the patch and skin up to temperatures of 80-120 °C for 8 hours until the patch is cured. Due to thermal mismatch between the boron and skin there is potential for residual stress. Consider the specific case of a patch applied to a complete panel which is surrounded by structure consisted of frames and sheet stringers bolted together. In this particular case it can be shown (see section A.5 in the Appendix A) that the residual stress is zero.

9.5 Operating temperatures

As mentioned in section 9.1 the maximum and minimum temperatures in this area are –67 °C and 120 °C respectively. The –67 °C temperature corresponds to the lowest airspeed and engine power that will maintain the aircraft in straight and level flight at Flight Level (FL) 500. In this condition the manoeuvre capability is limited. The maximum temperature corresponds to Mach 2 at FL 350. While the manoeuvre capability for the coldest temperature is limited, it is not necessary to use a load alleviation factor. Note that the relationship of shear modulus to temperature for FM300 is:

$$G = 415 - 1.8T \tag{70}$$

The damping material, Dyad 609, is most effective over the range of temperature 20-120 °C. At low temperatures the loss factor of the repair will only be 0.004. Available data indicates that the properties of Dyad 609 do not change at low temperatures. Hence at low temperatures the repair is not damped. The patch works as a 'stand off' repair at low temperatures. The thickness of the damping layer increases the bending stiffness sufficiently to reduce the stress intensity.

9.6 Results

Firstly consider an un-damped patch in Figure 24. This is a classic example that occurs when un-damped patches are used. One repair is a simple un-damped boron patch repair while the other is an un-damped aluminium patch. Both repairs result in stress intensity factors that will result in crack growth. The aluminium plate is bonded to the skin, but the adhesive softens with rise of operating temperature. Almost the same result will occur with a bolted plate although the softening will not occur, however the end result is much the same.

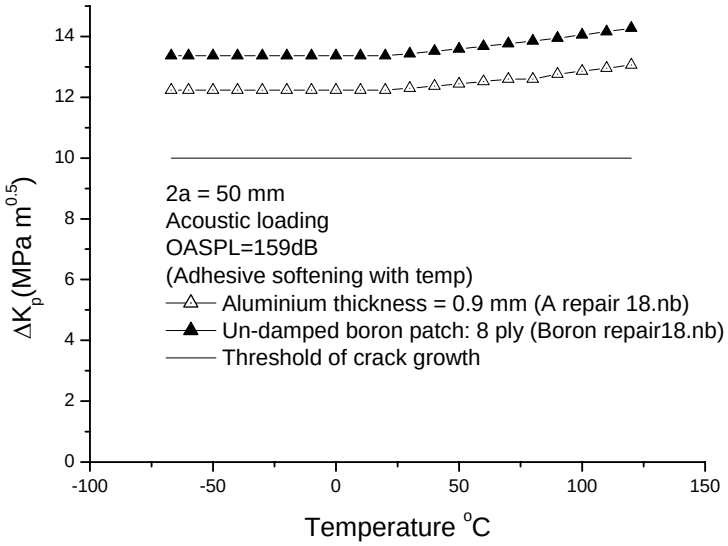

Figure 24: Predicted peak stress intensity factor versus operating temperature for un-damped boron repair ,8 plies, and un-damped aluminium plate repair

The results for the acoustic loading are shown in Figure 25 and indicate the performance of the 4, 6 and 8 layer designs. Note that the F.E. results for the 4 layer patch show good agreement with the analytic values. Clearly both the 6 and 8 ply designs survive this loading.

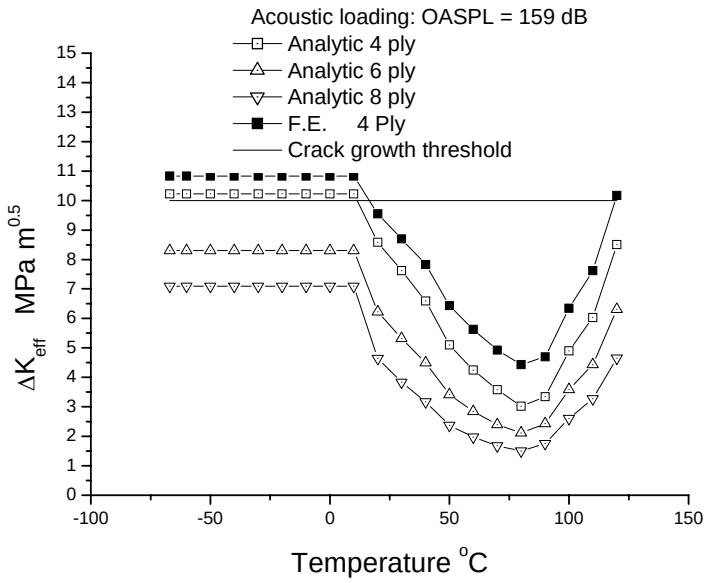

Figure 25: Predicted peak stress intensity factor versus operating temperature at OASPL=159 dB, using Dyad 609, for crack length 2a=50 mm. This corresponds to 4, 6 and 8 ply configuration.

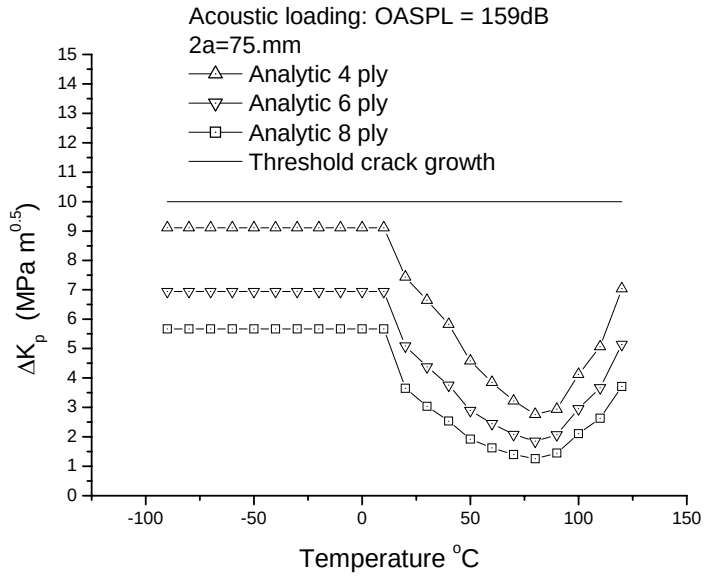

Figure 26: Predicted peak stress intensity factor versus operating temperature at OASPL=159 dB, using Dyad 609, for crack length 2a=75 mm. This corresponds to 4, 6 and 8 ply configuration.

It is known that as the crack grows the stress intensity in a panel, surrounded by structure, will decrease as the crack tip approaches the boundary, see Figure A6 in Appendix A. The

analysis is capable of predicting the change in stress intensity as the crack grows. This set up in Correction Tables, and also requires a Fortran program to compute the new stress intensity.

For a crack size of 2a=75 mm, the results are shown in Figure 26. All three designs for 4, 6 and 8 layers survive this loading. As the crack length extends to 2a=100 mm in Figure 27, and 2a=150mm in Figure 28 all designs survive. It is evident that the 6 layer is always below the threshold for crack growth. Hence a 6 layer design is practical since it is capable of stopping very large cracks, with no crack growth, and hence has an infinite fatigue life.

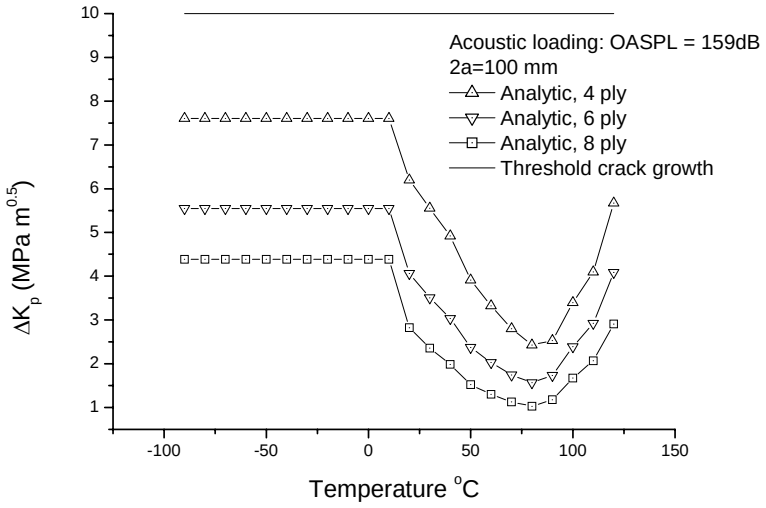

Figure 27: Predicted peak stress intensity factor versus operating temperature at OASPL=159 dB, using Dyad 609, for crack length 2a=100 mm. This corresponds to 4, 6 and 8 ply configuration.

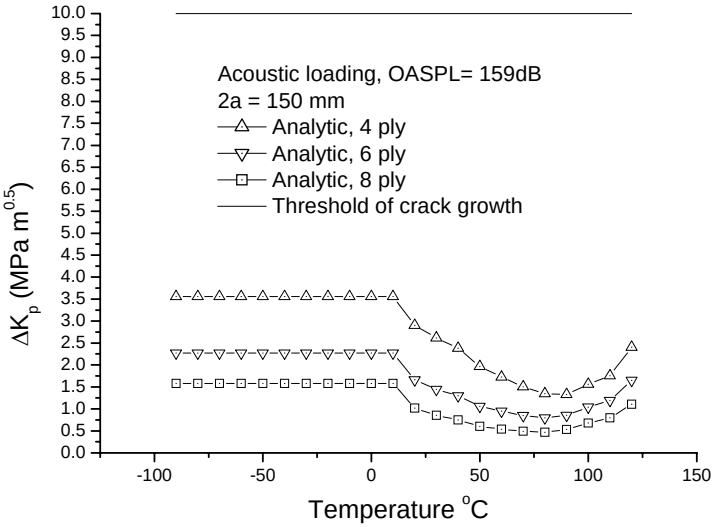

Figure 28: Predicted peak stress intensity factor versus operating temperature for damped repairs for 4, 6 and 8 ply lay-up. The crack length is 2a=150 mm.

Overall the results show that the analytical solution underestimates the F.E. results slightly at low temperatures and a safety factor 1.05 is needed. At high temperatures, a factor of 1.2 is required.

Data for all plotted results on Figures 25–28 are contained in Appendix A, Tables A10-24. All equations in this report have been solved using Mathematica.

Table 10: Configurations of repair

Mathematica file	Number of layers	Lay up
DampedRepair 609a.nb	4	0,90,90,0
DampedRepair 609a.nb	6	0,90,0,90,0,90
DampedRepair 609a.nb	8	0,90,0,90,90,0,90,0

Shown in Figure 29 is the predicted variation in rms strain in the plate versus operating temperatures for a 4, 6 and 8 ply configuration.

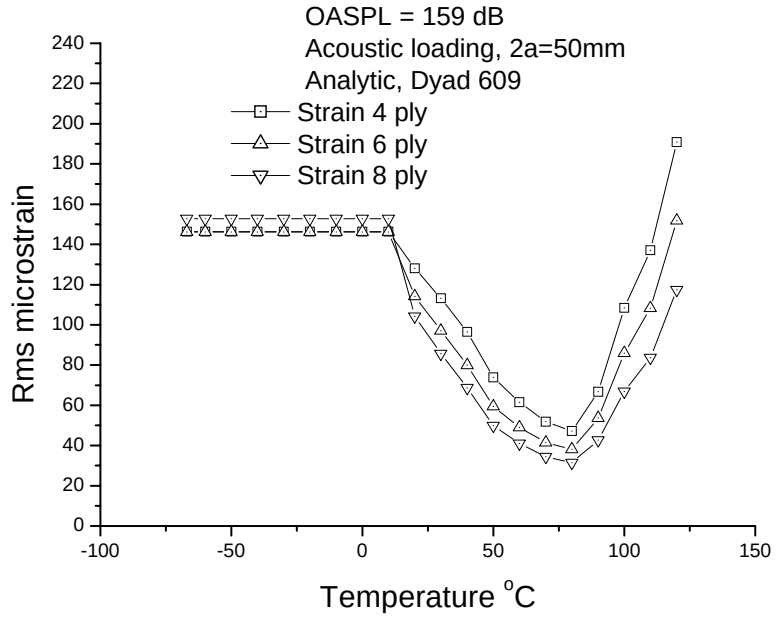

Figure 29: Residual predicted rms strain versus operating temperature at OASPL=159 dB, using Dyad 609, for crack length 2a=50 mm. This corresponds to 4, 6 and 8 ply configuration.

9.7 Strength of Dyad 609

Manufacturer's data for Sound Coat Dyad 609 gives the tensile strength as 17.2 MPa. Due to the environmental affects a knock down factor of 60 is used. The repair is located on the side of the fuselage and the edge is protected from erosion by sealant. Also the repair is located within the boundary layer. As a result, the largest suction that can be achieved is in a vacuum, i.e. 0.097 MPa. Hence the margin of safety is $17.2/(60\times 0.097)-1 = 1.96$

The only other source of loading would come from a sideslip resulting in compression loading. Assume a side-slipe angle of 45 degrees, the load for a speed of 700 m/s and for a patch of size 303x305 mm is $0.5\rho V^2 = 0.212MPa$. The margin of safety against compression is $17.2/(60\times 0.213) - 1 = 0.35$.

9.8 Cost savings using highly damped repairs

In Appendix B costs are given for the standard RAAF scab metal repair and the highly damped repair. These costs show that while damped repair was slightly lower in costs, lay-up of the boron / epoxy / Dyad609 repair contributes to the labour costs. Mass production would result in cost savings allowing patches to be cut out from large sheets of patch material. The main difference between the repairs is fatigue life. It has been shown in this report that with appropriate design the fatigue life of the damped repair can be infinite, while large metallic repairs operate above the threshold for crack growth and as a result need to be replaced frequently. Over a ten-year period the batch of 11 F/A-18's suffering from acoustic fatigue damage in the aft fuselage would probably cost $1.1 million for metallic scab repairs. In comparison the use of highly damped repairs could result in cost savings of one order of magnitude, compared to metal scab repairs.

10. Conclusions

A generic design procedure has been developed using a number of closed form solutions. These consist of a simplified dynamic analysis together with crack bridging theory. Furthermore, the solution is also applicable for plates containing cracks on the boundary, accounting for the effect of residual thermal stresses. The procedure uses crack growth equations which have been found to give good results for acoustic fatigue data. It has been shown that the analysis for crack bridging can predict the repair efficiency with all the plate edges being either simply supported or clamped. As a result, this generic design procedure will enable optimum design of highly damped repairs to acoustically-induced cracked panels. It has been found that a highly damped repair is a viable, low risk, low cost repair to prevent any crack growth on the aft fuselage of the F/A-18. This repair does not in any way place a performance limitation on the F/A-18. This repair would extend the life of this component of the F/A-18 beyond 6000 hours. Furthermore over a period of 10 years, the cost savings are one order of magnitude improvement than those for metallic repairs.

11. References

[1] A.A. Baker and R. Jones (Eds), Bonded Repair of Aircraft Structures. Martinus Nijhoff Publishers, The Hague, 1988.

[2] T.K. Brewer, A/B/C/D Aircraft Lower Nacelle Skin Acoustic and Strain Measurements and Sonic Fatigue Analysis. McDonnell Douglas Aerospace, MDC 94B0044, Mar, 1994.

[3] R.J. Callinan, S.C. Galea and S. Sanderson, Finite element analysis of bonded repairs to edge cracks in panels subjected to acoustic excitation. J. Comp. Struct., p649-660, 1997.

[4] RAAF Engineering Standard DEFAUST9005-A.

[5] R.J. Callinan, W.K. Chiu and S.C. Galea, Optimization of a Composite Repair to Cracked Panels Subjected to Acoustic Excitation. Paper A98-31631 21st ICAS Congress 13-18 Sept. 1998, Melbourne, Australia.

[6] L. Rogers, J. Maly, I.R. Searle, R.I. Begami, W. Owen, D. Smith, R.W. Gordan and D. Conley, Durability Patch: Repair and Life extension of high-cycle fatigue damage on secondary structure of ageing aircraft, 1ST Joint DOD/FAA/NASA Conference on Aging Aircraft, Ogden, Ut, 8-10 July, p595-623, 1997.

[7] S.L. Liguore, K. Hunter, R. Perez and T.H. Beier, Flight Test Evaluation of Damped Composite Repairs For Sonic Fatigue. Sonic Fatigue Session of the 40th AIAA/ASME/ASCE/AHS SDM Conference St. Louis, MO April 12-15, p1498-1508, 1999.

[8] R.W. Gordon, J.J. Hollkamp, S. Liguore and R.J. Callinan, An Experimental Investigation of Damped Repairs for Sonic Fatigue. Fifth Joint NASA/FAA/DoD Conference on Aging Aircraft, Sept. 2001.

[9] S.L. Liguore, T.H. Beier, R.W. Gordon and J.J. Hollkamp, Design and Analysis of Damped Repairs For Sonic Fatigue Cracking. The 2001 USAF Aircraft Structural Integrity Program Conference, 11-13 Dec. Williamsburg, Virginia, USA.

[10] R. Ikegami, E. Haugse and A. Trego, Structural Technology and Analysis Program. AFRL-VA-WP-TR-2001-3037, June 2001.

[11] R.J. Callinan, C.H. Wang, S.C. Galea, S. Sanderson and L.R.F. Rose, Analytical Solution for the Stress Intensity Factor in Bonded Repairs to Panels Subjected to Acoustic Excitation. Presented to joint FAA/DoD/NASA Conference on Aging aircraft. 20-23 Sept. 1999.

[12] D.J. Mead, Passive Vibration Control. John Wiley and Sons, 1982.

[13] E. E. Ungar, Chapter 12 Structural Damping. Noise and Vibration Control Engineering: Principles and Applications. Edit L. L. Beranck and I. L. Ver. John Wiley and Sons.

[14] Anon. Soundcoat data sheets for Dyad 606 and 609.

[15] H. Climent and J. Casalengua, Application of a PSD technique to acoustic fatigue Stress Calculations in Complex Structures. Symposium on ' Impact of Acoustic Loads on Aircraft Structures', Paper 12, AGARD-CP-549, Lillehammer, Norway, May 1994.

[16] L.R.F. Rose, Theoretical Analysis of Crack Patching, in Bonded Repair of Aircraft Structures, A.A. Baker and R. Jones (eds.), Martinus Nijhoff Publishers, The Hague, (1988).

[17] C.H. Wang and L.R.F. Rose, A crack bridging model for bonded plates subjected to tension and bending. Int. J. of Solids and Structures, Vol. 36, pp. 1985-2014, 1999.

[18] C.H. Wang, L.R.F. Rose and R.J. Callinan, Analysis of Out-of-Plane Bending in One-Sided Repair. Int. J. Solids Structures, Vol. 35, No. 14, p 1653-1675, 1998.

[19] B.L. Clarkson, Stresses in Skin Panels Subjected to Random Acoustic Loading. The Aeron. Jour., Vol 72, No 695, p1000-1010, Nov. 1968.

[20] J.W. Miles, On Structural Fatigue Under Random Loading. J. Aeron. Sci., Vol 21, No 11, p753-762, Nov. 1954.

[21] L.W. Lassiter and R.W. Hess, Calculated and Measured stresses in simple panels subject to intense Random Acoustic Loading Including the near noise field of a turbojet engine. NACA Tech. Note 4076, Sept. 1957.

[22] K.P. Byrne, On the Growth Rate of Bending Induced Edge Cracks in Acoustically Excited Panels. J. Sound and Vibration, 1977, 53(4) 505-528.

[23] C.M. Harris Edit., Shock and Vibration Hanbook, Third edition McGraw-Hill, 1961.

[24] W.C. Young, Roark's Formulas for stress and strain. Sixth Edition, McGraw-Hill, 1989.

[25] L.R.F. Rose, A Cracked Plate Repaired by Bonded Reinforcements. Int. Journ. of Fracture, 18 (1982) 135-144.

[26] Anon, FM300 Film adhesive. Manufactures data. Cytec Fiberite Inc. S. Barlow

[27] K.P. Byrne, Strains Affecting the Growth Rate of Edge Cracks in Acoustically Excited Panels. ISVR Tech. Rep. 59, Nov, 1972.

[28] L. Schwarmann, Material Data of High-Strength Aluminium Alloys for Durability Evaluation of Structures. Aluminium-Verlag, Dusseldorf, 1988.

[29] R.J. Callinan, C.H. Wang, A. Rider and S. Tejedor, Experimental Work carried out to Evaluate the Effectiveness of Highly Damped Repairs. DSTO-TN-0589, AR-013-234, 2005.

[30] K. P. Byrne, Bending Induced Crack Propagation in Bare and Clad 4% Cu-Aluminium Alloys with Reference to Acoustically Propagated Fatigue Cracks. Institute of Sound and Vibration Research. University of Southhampton, Technical Report No. 61, Aug. 1973.

[31] R.J. Callinan, P. Ferrarotto, R. Geddes, I. Stoyanokski and S. Tejeddor, Flight Trial of Dosimeter on F/A-18 to Determine the Acoustic Environment and the Effectiveness of the Highly Damped Patch. Draft DSTO Report DSTO-RR-0284, AR 013-232.

[32] R.J. Callinan, S. Sanderson, T. Tran-Cong, and K. Walker. Development and Validation of a Finite Element Based Method to Determine Thermally Induced Stresses in Bonded Joints of Dissimilar Materials.DSTO-RR-0109, Jun, 1997.

[33] S. Barlow. Determination of F/A-18 Thermal Profile, AR-009-066, July 1995.

[34] Advances in the Bonded Composite Repair of Metallic Aircraft Structure. Ed. A.A. Baker, L.R.F. Rose, R. Jones, Elsevier, 2002.

[35] Duong, C. N. and Wang, C. H. (2006) *Composite repair – theory and design*, Elsevier.

Appendix A: Validation Studies

A.1. Validation of un-repaired panel

This section provides the validation of the closed form solution using both experimental and F.E. results. The latter involves the use of the random vibration capability of the NASTRAN F.E. program. Furthermore the experimental data used to validate the closed form solution was from flight trials [31].

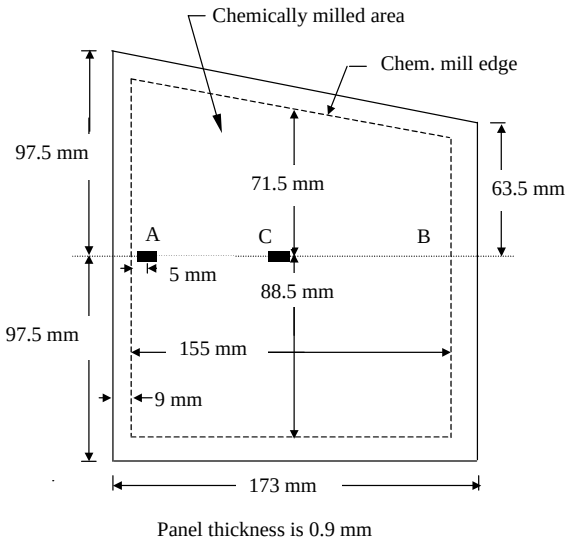

Figure A1: Dimensions of panel and dotted outline of chemical milled area

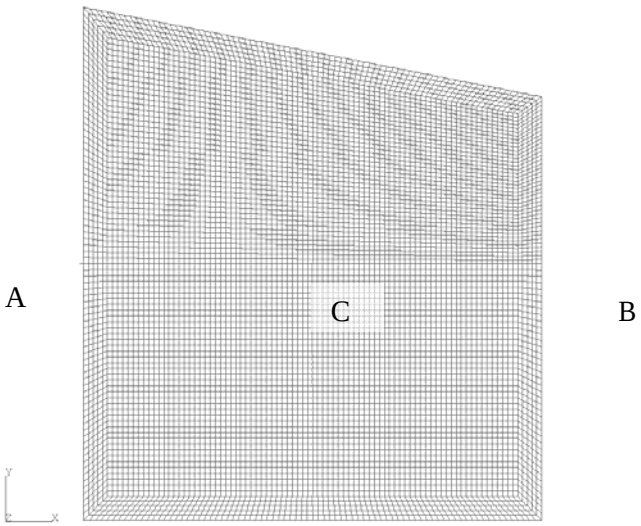

Figure A2: F.E. model of un-patched panel

The dimensions of plate to be considered are shown in Figure A1. The corresponding F.E. mesh is shown in Figure A2 has been used for comparison purposes. This geometry is similar to a panel on the F/A-18 aft fuselage where acoustic fatigue cracking has been found. The geometry has been simplified, but contains a chemically milled region. Also a land outer area exists which is thicker than the chemically milled region. This region is fastened to the stiffener with one or two lines of rivets. The outer boundary in Figure A2 coincides with the rivet lines.

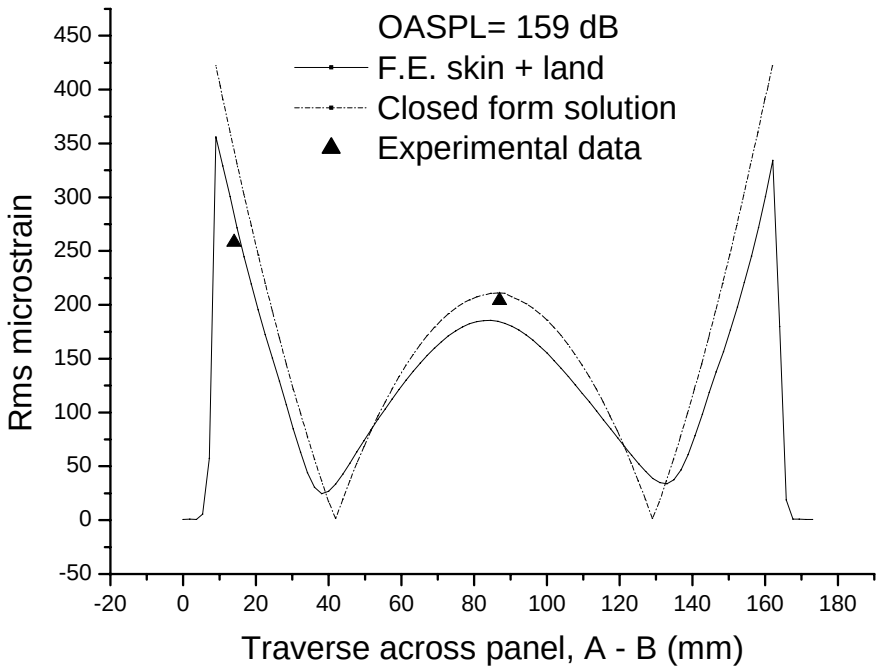

Figure A3: Rms microstrain for un-patched panel, versus distance across the panel

The results shown in Figure A3 correspond to the F.E. mesh which is shown in Figure A2. These results show the comparison of the closed form solution, F.E. and flight trial data points. The overall sound pressure level, OASPL, is determined by matching the closed form solution and the experimental data at the centre of the plate. The F.E. results determined at the calculated OASPL agree well with the closed form solution, hence the experimental data. At the edge of the plate the closed form solution slightly over estimates the flight trial data point, while the F.E. slightly under estimates the closed form solution. Overall the agreement between the closed form, F.E. and flight data is good. As a result the loading to achieve these was an OASPL of 159 dB. Results are also shown in Table A1, and good comparisons have been made for parameters such as frequency, lateral displacement and stress intensity factor. The value of the lateral displacement indicates that a linear solution is acceptable. The F.E. model includes the chemically milled area together with the land.

Table A1: F.E. validation models for panel, at OASPL=159dB, loss factor = 3.2%

Model	Frequency F.E.	Frequency closec (Hz)	F.E. Lateral Displ.	Closed Lateral displ	F.E. strain at edge of Panel microstrain	Closed form Strain microstrain
Chem. mill	324.4	328.8	0.673	0.761	427.4	389.5
Skin+land	374.6	328.8	0.692	0.761	340.5	389.5

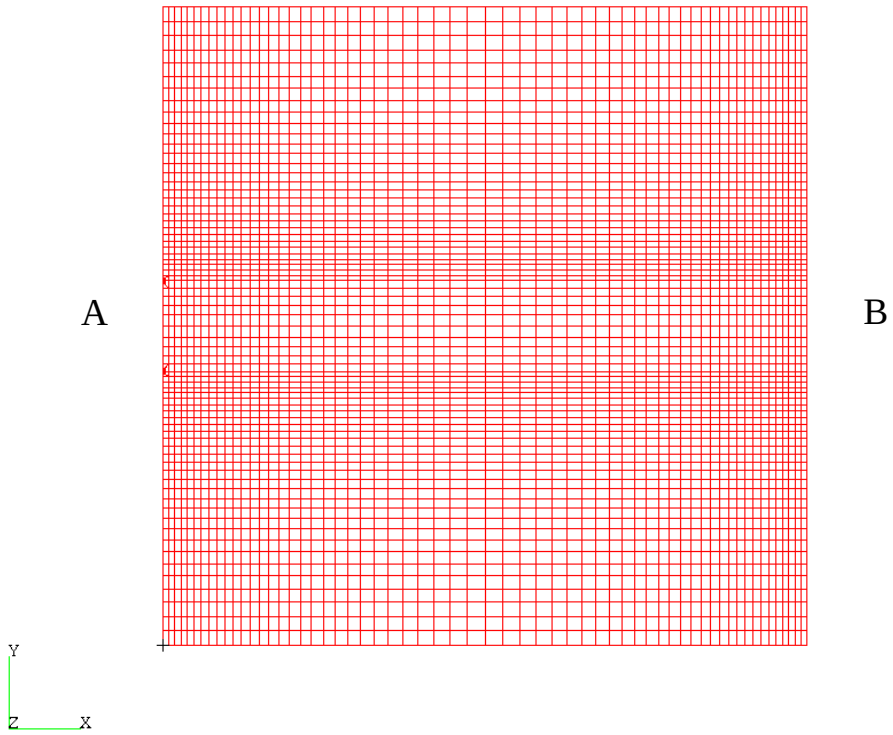

Figure A4: F.E. mesh density for chemically milled model to validate a closed form solution for the patched model, using Dyad 606. Dimensions are 175 mm by 176 mm.

A.2. Validation of repaired panel

The second part of the validation, now knowing the sound pressure level, was to predict the microstrain and compute the stress intensity for a repaired plate. The mesh is shown in Figure A4 and the results are shown in Figure A5. Firstly for comparison purposes no crack exists in the reinforced plate. In this particular case both the F.E. and closed form solution under estimate the microstrain. Secondly the crack is introduced. The results shown in Table A2 cover the cracked and un-cracked case. These results show good agreement for frequency and lateral displacement. The stress intensity factor is over predicted and hence conservative for a

SPL of 159 dB. It should be noted that while the test flight value of the repaired plate strain at the edge of the plate for flight 1 was 87 rms microstrain, for flights 2 and 4 was 83 and 72 microstrain respectively. Overall these results have shown a good correlation with test flight strains.

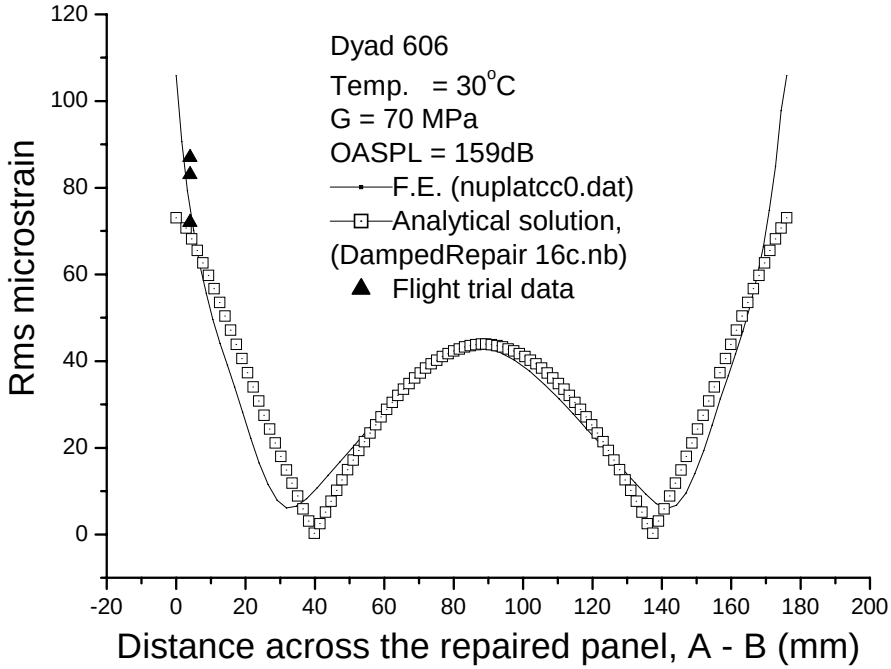

Figure A5. Distance across the repair (A to B) versus rms microstrain

Table A2. F.E. validation model for repaired panel with crack,2a=25.4, OASPL=159 dB, Dyad 606, load factor L=1.

Temp °C	Freq. F.E. (Hz) No crack	Freq. Closed (Hz)	F.E. Lateral Disp(mm) rms	Closed Lateral Disp (mm) rms	K_{peak} F.E. (MPa $m^{0.5}$)	K_{peak} Closed form (MPa $m^{0.5}$)
30	560.7	571.5	0.1159 *nuplatcc.dat *nuplatcc.db	0.08714	4.277 nuplatee.dat nuplatee.db	3.689
50	314.0	314.8	0.14218 *nuplatdd.dat *nuplatdd.db	0.1245	3.163 nuplataa.dat nuplataa.db	2.258

* No crack.

F.E. model in which crack exists is nuplataa.db, nuplataa.dat, nuplatee.db, nuplatee.dat

Table A3: Extension of Table A2

Shear Modulus (Mpa)	Loss factor	microstrain	fmm	fbm	fbb	fmb
70	0.115545	72.9269	0.1697	5.3280E-2	5.9360E-2	7.8215E-3
5	0.394547	68.1903	0.18962	3.78565E-2	3.55668E-3	7.8963E-2

Table A4: Extension of Table A2

Material loss factor	**Load factor L	Program	COD (mm)	F.E. data file	Crack tip Size (mm)
0.330	1.000	*DampedRepair 16cca.nb	1.5284E-7	nuplatee.dat	0.06314
1.000	1.000	*DampedRepair 16cca.nb	1.1298E-7	nuplataa.dat	0.06314

** load factor L= 1.0, *Mathematica file.
(See peak value in Figure 27)

For the F.E. analysis the stress intensity factor is calculated using a crack opening displacement formula for plane stress:

$$K_{rms} = \frac{E\,V}{4}\sqrt{\frac{2\pi}{l}} \qquad \text{(A1)}$$

where l is the length of the crack-tip element
V is the in-plane displacement at distance l from the crack-tip
E is Young's modulus

The calculation of the stress intensity indicates the effect of boundary conditions on the repair. The difference between the experimental and calculated strains is most likely due to edge constraint conditions. The higher experimental values result from the repair extending just outside the rivet line. If the repair on the flight trial aircraft were extended further into the adjacent panel, lower edge strains would have been recorded. F.E. analysis has shown that it is only necessary to extend the repair across the land region adjacent to the crack.

A.3. Correction factors

There is some disagreement between the calculation of stress intensity between F.E. and closed form solution. This is partly due to the simplification of the crack bridging theory in that the crack is normally considered at the centre of the panel rather than at the edge. The F.E. result is the most accurate. The stress intensity factor has been evaluated at both the centre and at the edge of the plate by F.E. and closed form solution for crack lengths of 2a=25.4 and 76.2 mm, see Table A5. For our case the value has been interpolated for 2a=50 mm. However the results for the comparison of stress intensity factors given in Table A2 do not justify a correction factor.

Table A5: Correction factor derived from F.E. analysis, for stress intensity factor, for repaired panel where G=70.MPa

Crack length (2a)	Centre of panel	Edge of panel	Ratio: centre / edge	Correction factor
25.4	3.177 cencrack.dat, -	3.2879 nuplataa.dat nuplataa.db	0.9663	0.9663 / 2=0.4831
76.2	3.534 cencrack5.dat, cenplat83.db	5.718 cencrack5.dat cenplat86.db	0.618	0.618 / 2=0.309
152.4	1.0456 cencrack0.dat cenplat158.db	1.459 cencrack1.dat cencrack159.db	0.716	0.760 / 2=0.358

Interpolated value for 2a=50.8 mm gives a correction factor of 0.673.

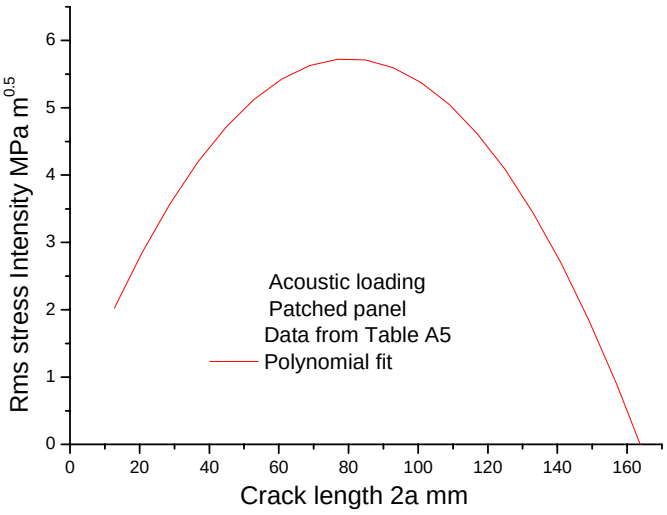

Figure A6: Data from Table A5, crack length versus stress intensity for edge crack

The data from Table A5 for the stress intensity at the edge of the plate has been plotted in Figure A6. A crack length of 2a = 50 mm corresponds to a stress intensity of 5 MPa m $^{0.5}$ .As the crack grows beyond 2a=76.2 mm, the stress intensity value of 5 MPa m $^{0.5}$ corresponds to a crack length of 2a=110 mm. If the crack length of 2a=50 mm is survivable, then beyond a crack length of 2a=110 mm no crack growth will occur.

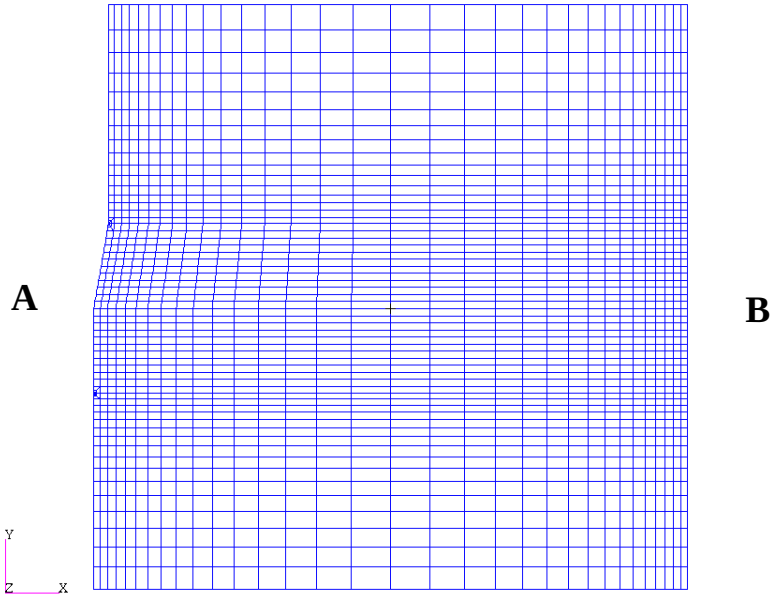

Figure A7: F.E. mesh density for chemically milled model to validate a closed form solution for the patched model, using Dyad 606. This mesh contains a 2a=50 mm crack.

A.4. Precise F.E. model for repaired panel

A large 50 mm crack is shown in the mesh in Figure A7. The geometry for this mesh is more precise than that in Figure A4, but with a larger crack. A traverse from A-B for strain is shown in Figure A8. In comparison to Figure A5 the strain in the centre of the plate has collapsed. Also the strain near the crack is very low while the strain in the plate on the opposite side of the crack is slightly increased. The stress intensity predicted from the closed form solution agrees with the crack opening displacement result using F.E. for the upper crack tip. However the predicted stress intensity for each crack tip are slightly different. A change in geometry as shown in Table A6 i.e. *a=173* and *a=178 mm*, does not significantly change the result for the closed form solution. While no validation for Dyad 609 has been carried out in Appendix A, results shown in Figure 27a (Page 34) show very good agreement in comparison to F.E. results.

Table A6: F.E./closed form solution for repaired panel with crack, OASPL=159 dB, Dyad 606, 2a=50 mm, 4 layers, see Figure A6.

a (mm)	b (mm)	G (MPa)	$f_{F.E.}$ (Hz)	f_{closed} (Hz)	v LHS (cod) mm	v RHS (cod) mm	K_{peak} LHS F.E. (MPa $m^{0.5}$)	K_{peak} RHS F.E. (MPa $m^{0.5}$)	K_{peak} Closed form (MPa $m^{0.5}$)
176.	175	70	531.	485.	1.33E-7	1.05E-7	2.875	3.610	3.632
173.	175	70		508.	-	-	-	-	3.673
178	175	70		471.	-	-	-	-	3.598

(Mathematica file: DampedRepair 16.nb)

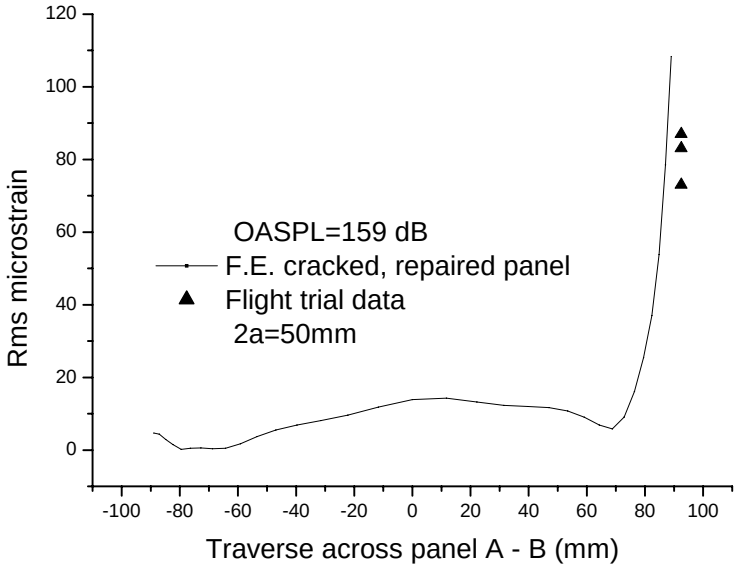

Figure A8: Distance across the repair (A to B) versus rms microstrain for 50 mm crack

Also contained in Tables A2, A3, A5, A6, A7 are all files used for the validation. This includes PATRAN databaseses, NASTRAN data files and Mathematica files. These are for the case of no-repair for the chemically milled panel, no chemical milling and the repaired case for which has only chemical milling. Mathematica users data shown in Tables A11 –A23.

Table A7: Numerical comparison of orthotropic response for simple test specimen and contains stresses

Layup	File / database	σ_x boron	δ_X	δ_Y
0,90,90,0 One single element through thickness (Homogenous)	Valid3a	Max=1.61E3 Min=7.50E2	2.89	1.84E-2
0,0,0,0 One single element through thickness (Homogenous)	Valid3b	Max=1.69E3 Min=7.69E2	1.88	4.86E-2
0,90,90,0 Four individual Elements through thickness	Valid4a	Max=1.66E3 Min=7.41E2	2.89	1.84E-2
90,0,0,90 One single element through thickness (Homogenous)	Valid3a	Max=2.97E3 Min=1.24E2	2.89	1.81E-2

A.5. Simple test problem

To demonstrate the PATRAN composite lay up capability, it was necessary to create a small test problem (Figure A9). This consists of a simple beam with various lay ups shown in Table 7. The model consists of skin, damping layer and boron constraining layer. This is loaded by an axial load at the end of the beam, and is also constrained at the other. The results for different lay ups are shown in Table A7. Also the cases of either one element or four elements per layer are shown.

Results in Table A7, for either one or four elements per layer, show a very small difference in stresses and displacements. (This validates the approach taken for the acoustically loaded panel in which two layers of boron are used). Note also that the 90,0,0,90 laminate has increased the stresses. To repair a acoustic panel where the crack is on the longest side of the panel, the 0,90,90,0 lay up should be used. The imbalance will be significantly reduced as the number of plies increases i.e. laminates of 6 plies or greater.

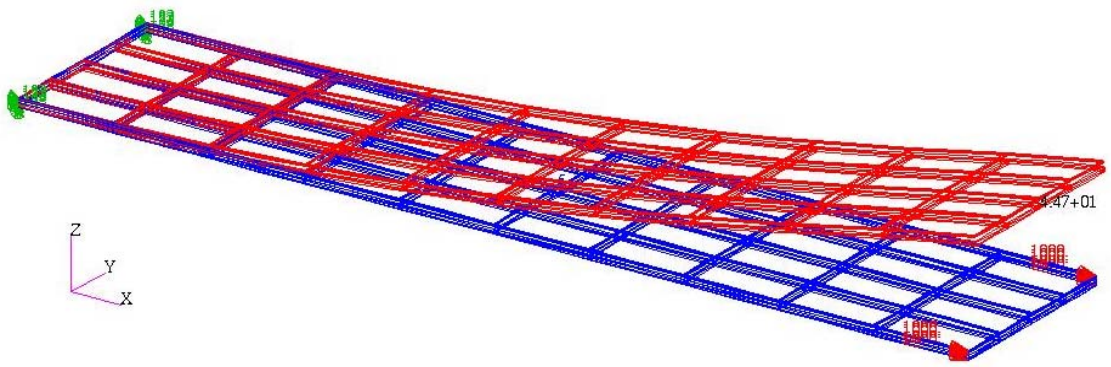

Figure A9: Small beam with pressure applied at one end and constrained at the other end

Table A8: Additional data for Table A7

Layup	δ_X	δ_Y
0,90,90,0 One single element through thickness	2.89	1.84E-2
0,0,0,0		
Four individual elements through thickness	2.89	1.84E-2
90,0,0,90	2.89	1.81E-2

A.6. Validation of zero residual stresses after cure

Consider a circular patch on a circular plate. In this case the radius of the patch is R_I and and the plate R_O. In our case $R_I = R_O$ since the repair overlaps the entire panel then clamped boundary conditions are applicable. From ref(52), equ(30) for the stress under the repair for cooling down after the cure is given by:

$$\sigma_1 = \frac{E_1}{(1-v)}\left[-\alpha_1 T_I + \frac{u}{R_I}\right] \tag{A3.1}$$

were u is the displacement at the edge of the patch . In our case $u = 0$. and due to cooling $T_I = -T_I$ hence we obtain:

$$\sigma_1 = \alpha_1 \, T_I \, \frac{E_1}{(1-v)} \tag{A3.2}$$

For the case of heating the plate alone to cure temperature, from [32]:

$$\sigma_1 = -0.5\,\alpha_1 E_1\left[T_I + \frac{(1+v)}{(1-v)}\right]\left[T_I + \frac{T_O - T_I}{2\ln(R_I/R_O)}\left[\left[\frac{R_I}{R_O}\right]^2 - 1\right]\right] \tag{A3.3}$$

This solution does not work where $R_I = R_O$, however if R_I is set $= 0.994 R_O$ then a good solution will be obtained. The temperature in the patch is T_O while the temperature at the boundary is T_I.

The residual stress is thus:

$$\sigma_R = -0.5\,\alpha_1 E_1\left[T_I + \frac{(1+v)}{(1-v)}\right]\left[T_I + \frac{T_O - T_I}{2\ln(R_I/R_O)}\left[\left[\frac{R_I}{R_O}\right]^2 - 1\right]\right] + \alpha_1 \, T_I \, \frac{E_1}{(1-v)} \tag{A3.4}$$

To determine the residual stress requires the addition of equations (A3.2 and A3.3), hence equation (A3.4). It has been found numerically that the sum of stresses cancel out with virtuality no residual stress remaining, see Table A9. Also the residual stress has been computed for a range of poison's ratio and has been shown to be very small. This exercise has been simply to demonstrate that in this case residual stresses due bonding will be zero.

Table A9: Residual stresses after cure from 100 °C. E_1 = 71000 MPa, $\alpha_1 = 23x10^{-6}$

R_O (mm)	R_O / R_I	T_I °C	T_O °C	EquA3.1 (MPa)	EquA3.3 (MPa)	Residual EquA3.4 (MPa)
88.0	1.006	100	0.0	-233.5	233.2	0.3

*Table A10: K/s Dyad 609, t = 1.016 mm, 8 plies, 2a=50 mm. *(DampedRepair16e_609c.nb)*

Temp °C	G	fmm	fbm	fbb	fmb	5.*K_{max}	L.F.
-67	300	0.14125	0.00622	0.04417	0.00625	7.38932	0.00867206
-60	300	0.14125	0.00622	0.04417	0.00625	7.38932	0.00867206
-50	300	0.14125	0.00622	0.04417	0.00625	7.38932	0.00867206
-40	300	0.14125	0.00622	0.04417	0.00625	7.38932	0.00867206
-30	300	0.14125	0.00622	0.04417	0.00625	7.38932	0.00867206
-20	300	0.14125	0.00622	0.04417	0.00625	7.38932	0.00867206
-10	300	0.14125	0.00622	0.04417	0.00625	7.38932	0.00867206
0	300	0.14125	0.00622	0.04417	0.00625	7.38932	0.00867206
10	300	0.14125	0.00622	0.04417	0.00625	7.38932	0.00867206
20	300	0.14125	0.00622	0.04417	0.00625	4.6398	0.021966
30	280	0.14299	0.00576	0.0446	0.00623	3.83528	0.0325334
40	200	0.15164	0.00341	0.04672	0.00607	3.16572	0.0512345
50	130	0.16293	0.00151	0.04955	0.00590	2.36655	0.0991672
60	85	0.17415	-0.00329	0.05246	0.00567	1.97901	0.15338
70	50	0.18800	-0.00778	0.05628	0.00534	1.67625	0.15338
80	25	0.20523	-0.01369	0.06155	0.00483	1.49853	0.335782
90	5	0.23825	-0.02547	0.07496	0.00349	1.75494	0.302044
100	1.7	0.25361	-0.03040	0.08464	0.00263	2.60597	0.147147
110	1.0	0.25929	-0.03181	0.08952	0.00225	3.27513	0.0982069
120	0.9	0.26029	-0.03014	0.09049	0.00297	4.65097	0.050208

*Mathematica file

Table A11: Loss factor components for Dyad 609, corresponding Table A10, h=1.016 mm, 2a=50 mm

Temp °C	η_C	η_1	η_3	$\mu\varepsilon_{rms}$	K_{peak}	f(Hz)
-67	0.004	.026	.004	165.98	7.0907	813.954
-60	0.004	.026	.004	165.98	7.0907	813.954
-50	0.004	.026	.004	165.98	7.0907	813.954
-40	0.004	.026	.004	165.98	7.0907	813.954
-30	0.004	.026	.004	165.98	7.0907	813.954
-20	0.004	.026	.004	165.98	7.0907	813.954
-10	0.004	.026	.004	165.98	7.0907	813.954
0	0.004	.026	.004	165.98	7.0907	813.954
10	0.004	.026	.004	165.98	7.0907	813.954
20	0.100	.026	.004	104.22	4.6398	814.258
30	0.170	.026	.004	85.6162	3.8353	811.039
40	0.240	.026	.004	68.7329	3.1657	790.063
50	0.400	.026	.004	49.9203	2.3666	759.343
60	0.522	.026	.004	40.9631	1.9790	721.027
70	0.677	.026	.004	34.44	1.6763	663.144
80	0.850	.026	.004	31.492	1.4985	573.987
90	1.042	.026	.004	42.7501	1.7549	403.008
100	1.000	.026	.004	66.9118	2.6060	355.326
110	1.000	.026	.004	83.6649	3.2751	344.257
120	0.500	.026	.004	117.462	4.6510	342.496

Table A12: Crack bridging data for Dyad 609, t = 0.762mm, 6 plies, 2a=50 mm.
**(DampedRepair16e_609b.nb)*

Temp °C	G	fmm	fbm	fbb	fmb	Loss.Fac.
-67	300	0.15867	0.03457	0.04737	0.008913	0.0134776
-60	300	0.15867	0.03457	0.04737	0.008913	0.0134776
-50	300	0.15867	0.03457	0.04737	0.008913	0.0134776
-40	300	0.15867	0.03457	0.04737	0.008913	0.0134776
-30	300	0.15867	0.03457	0.04737	0.008913	0.0134776
-20	300	0.15867	0.03457	0.04737	0.008913	0.0134776
-10	300	0.15867	0.03457	0.04737	0.008913	0.0134776
0	300	0.15867	0.03457	0.04737	0.008913	0.0134776
10	300	0.15867	0.03457	0.04737	0.008913	0.0134776
20	300	0.15867	0.03457	0.04737	0.008913	0.0260082
30	280	0.16041	0.03447	0.04781	0.008876	0.0360016
40	200	0.16890	0.03388	0.04999	0.008672	0.0540161
50	130	0.17977	0.03286	0.05290	0.008357	0.100668
60	85	0.19032	0.03157	0.05589	0.007199	0.154953
70	50	0.20299	0.02963	0.05978	0.007464	0.240213
80	25	0.21831	0.02662	0.06516	0.006685	0.354973
90	5	0.24630	0.01872	0.07876	0.004728	0.368612
100	1.7	0.25884	0.01372	0.08853	0.003518	0.194661
110	1.0	0.26196	0.01260	0.09175	0.003168	0.133074
120	0.9	0.26423	0.01113	0.09442	0.0028959	0.068694

*Mathematica file

Table A13: Loss factor components, Dyad 609, corresponding Table A13, h=0.762 mm, 2a=50 mm.

Temp °C	η_C	η_1	η_3	$\mu\varepsilon_{rms}$	K_{peak}	f(Hz)
-67	0.004	.026	.004	158.709	8.3011	735.006
-60	0.004	.026	.004	158.709	8.3011	735.006
-50	0.004	.026	.004	158.709	8.3011	735.006
-40	0.004	.026	.004	158.709	8.3011	735.006
-30	0.004	.026	.004	158.709	8.3011	735.006
-20	0.004	.026	.004	158.709	8.3011	735.006
-10	0.004	.026	.004	158.709	8.3011	735.006
0	0.004	.026	.004	158.709	8.3011	735.006
10	0.004	.026	.004	158.709	8.3011	735.006
20	0.100	.026	.004	114.173	6.2233	735.281
30	0.170	.026	.004	97.0556	5.3198	732.561
40	0.240	.026	.004	79.9758	4.4903	714.646
50	0.400	.026	.004	59.3936	3.4111	688.243
60	0.522	.026	.004	49.0792	2.8438	654.859
70	0.677	.026	.004	41.4192	2.3965	603.387
80	0.850	.026	.004	38.0504	2.1134	520.961
90	1.042	.026	.004	53.5769	2.4318	349.628
100	1.000	.026	.004	85.979	3.5892	297.963
110	1.000	.026	.004	108.312	4.4346	285.657
120	0.500	.026	.004	151.844	6.3139	283.665

*Table A14: K/s Dyad 609, t = 0.508 mm, 4 plies, 2a=50 mm. *(DampedRepair16e_609a.nb)*

Temp °C	G	fmm	fbm	fbb	fmb	$5*K_{max}$
-67	300	0.18288	0.078155	0.05329	0.013469	10.6560
-60	300	0.18288	0.078155	0.05329	0.013469	10.6560
-50	300	0.18288	0.078155	0.05329	0.013469	10.6560
-40	300	0.18288	0.078155	0.05329	0.013469	10.6560
-30	300	0.18288	0.078155	0.05329	0.013469	10.6560
-20	300	0.18288	0.078155	0.05329	0.013469	10.6560
-10	300	0.18288	0.078155	0.05329	0.013469	10.6560
0	300	0.18288	0.078155	0.05329	0.013469	10.6560
10	300	0.18288	0.078155	0.05329	0.013469	10.6560
20	300	0.18288	0.078155	0.05329	0.013469	8.5883
30	280	0.18445	0.078370	0.053730	0.013394	7.6214
40	200	0.19197	0.079259	0.055927	0.012989	6.5905
50	130	0.20133	0.079969	0.058829	0.012394	5.1014
60	85	0.21015	0.080177	0.06179	0.011731	4.2456
70	50	0.22805	0.079738	0.06566	0.010821	3.5784
80	25	0.23251	0.078027	0.07097	0.009542	3.0151
90	5	0.25385	0.069948	0.08445	0.006558	3.3472
100	1.7	0.26331	0.062442	0.09414	0.004813	4.8870
110	1.0	0.26567	0.059840	0.09733	0.004318	6.0325
120	0.9	0.26741	0.057688	0.09998	0.003935	8.5032

*Mathematica file

Table A15: Further props.: Dyad 609, corresponding TableA16, h=0.508 mm, 2a=50 mm.

Temp °C	η_C	η_1	η_3	Loss.F	$\mu\varepsilon_{rms}$	K_{peak}	f(Hz)
-67	0.004	.026	.004	.0198976	158.861	10.2260	647.632
-60	0.004	.026	.004	.0198976	158.861	10.2260	647.632
-50	0.004	.026	.004	.0198976	158.861	10.2260	647.632
-40	0.004	.026	.004	.0198976	158.861	10.2260	647.632
-30	0.004	.026	.004	.0198976	158.861	10.2260	647.632
-20	0.004	.026	.004	.0198976	158.861	10.2260	647.632
-10	0.004	.026	.004	.0198976	158.861	10.2260	647.632
0	0.004	.026	.004	.0198976	158.861	10.2260	647.632
10	0.004	.026	.004	.0198976	158.861	10.2260	647.632
20	0.100	.026	.004	.0305986	128.027	8.5883	647.859
30	0.170	.026	.004	.0391693	113.193	7.6214	645.835
40	0.240	.026	.004	.0549778	96.4419	6.5905	632.298
50	0.400	.026	.004	.0963854	73.8778	5.1014	612.196
60	0.522	.026	.004	.146113	61.5286	4.2456	586.322
70	0.677	.026	.004	.227325	51.8775	3.5784	545.341
80	0.850	.026	.004	.346056	47.2442	3.0151	476.057
90	1.042	.026	.004	.409403	66.6844	3.3472	315.022
100	1.000	.026	.004	.233752	108.418	4.8970	261.868
110	1.000	.026	.004	.163993	137.056	6.0325	248.907
120	0.500	.026	.004	.086328	190.856	8.5032	246.756

Table A16: K/s Dyad 606, t = 0.508 mm, 4 plies, 2a=25.4 mm.

Temp °C	G	fmm	fbm	fmb	Fbb	Loss Factor
-40	300	0.15240	0.05753	0.01015	0.05042	0.01952 -
-20	300	0.15240	0.05753	0.01015	0.05042	0.01953
0	300	0.16583	0.05465	0.00841	0.05709	0.01953
10	100	0.16583	0.05465	0.00841	0.05709	0.01998
30	70	0.16907	5.329E-2	7.822E-2	5.937E-2	0.1746
40	17	0.18166	4.626E-2	5.523E-3	6.885E-2	0.4195
50	5.	0.18863	0.03917	0.00382	0.07740	0.3953
60	1.5	0.19308	0.03220	0.00253	0.08569	0.1189
70	0.60	0.19530	0.02727	0.00180	0.09167	0.0400
80	0.40	0.19604	0.02523	0.00154	0.09419	0.0242

Table A17: F.E. structural results for 4 ply repair, mesh shown in Figure A6

Temp °C	G (MPa)	COD top (mm)	COD bot (mm)	Ktop (MPa $m^{0.5}$)	Kbot (MPa $m^{0.5}$)	Kave (MPa $m^{0.5}$)
-67	300	2.5679E-4	2.0528E-4	1.3944	1.1231	1.2587
-60	300	2.7887E-4	2.2294E-4	1.5143	1.2197	1.3670
-50	300	3.0745E-4	2.4579E-4	1.6694	1.3447	1.5071
-40	300	3.3368E-4	2.6676E-4	1.8119	1.4594	1.6357
-30	300	3.5799E-4	2.8620E-4	1.9439	1.5658	1.7548
-20	300	3.8068E-4	3.0434E-4	2.0671	1.6650	1.8660
-10	300	4.0216E-4	3.2151E-4	2.1837	1.7589	1.9713
0	300	4.2248E-4	3.3775E-4	2.2940	1.8478	2.0709
10	300	4.4193E-4	3.5331E-4	2.3997	1.9329	2.1663
20	300	3.8943E-4	3.1163E-4	2.1146	1.7049	1.9098
30	280	3.5432E-4	2.8414E-4	1.9239	1.5545	1.7392
40	200	3.1802E-4	2.5705E-4	1.7268	1.4063	1.5666
50	130	2.5979E-4	2.1260E-4	1.4107	1.1631	1.2869
60	85	2.2609E-4	1.8719E-4	1.2277	1.0241	1.1259
70	50	1.9693E-4	1.6477E-4	1.0693	0.9014	0.9854
80	25	1.7646E-4	1.4871E-4	0.9582	0.8136	0.8859
90	5	1.8990E-4	1.5482E-4	1.0312	0.8470	0.9391
100	1.7	2.6363E-4	2.0210E-4	1.4315	1.1057	1.2686
110	1.0	3.2044E-4	2.3872E-4	1.7400	1.3060	1.5230
120	0.9	4.3053E-4	3.1678E-4	2.3378	1.7331	2.0355

*Top crack tip size = 0.06714 mm, node=20415

*Bottom crack tip size = 0.06614 mm, node=20521

Table A18: F.E. structural results for 4 ply repair, mesh shown in Figure A6

Temp °C	$K_p = 5*K_{max}$ (MPa $m^{0.5}$)	File
-67	10.8315	rjc01.dat
-60	10.8315	rjc01.dat
-50	10.8315	rjc01.dat
-40	10.8315	rjc01.dat
-30	10.8315	rjc01.dat
-20	10.8315	rjc01.dat
-10	10.8315	rjc01.dat
0	10.8315	rjc01.dat
10	10.8315	rjc02.dat
20	9.5482	rjc03.dat
30	8.6956	rjc04.dat
40	7.8324	rjc05.dat
50	6.4341	rjc06.dat
60	5.6291	rjc07.dat
70	4.9266	rjc08.dat
80	4.4291	rjc09.dat
90	4.6951	rjc10.dat
100	6.3426	rjc11.dat
110	7.6146	rjc12.dat
120	10.1765	rjc13.dat

rjc01.dat contains sub cases of load factors for PSD.

Table A19: F.E. Temperature results for 4 ply repair, mesh shown in Figure A6

Temp.^{o} C	Data files (NASTRAN)	COD_{top} (mm)	COD_{bot} (mm)	K_{top} MPa $m^{0.5}$	K_{bot} MPa $m^{0.5}$	K_{ther} MPa $m^{0.5}$
-67	temp_87.dat	5.5698E-3	4.7084E-3	30.2418	25.7581	28.0000
-60	temp_80.dat	5.1216E-3	4.3296E-3	27.8083	23.6858	25.7471
-50	temp_70.dat	4.4814E-3	3.7884E-3	24.3322	20.7251	22.5287
-40	temp_60.dat	3.8412E-3	3.2472E-3	20.8562	17.7643	19.3103
-30	temp_50.dat	3.2010E-3	2.7060E-3	17.3802	14.8036	16.0919
-20	temp_40.dat	2.5608E-3	2.1648E-3	13.9041	11.8429	12.8735
-10	temp_30.dat	1.9206E-3	1.6236E-3	10.4281	8.8822	9.6552
0	temp_20.dat	1.2804E-3	1.0824E-3	6.9521	5.9214	6.4368
10	temp_10.dat	6.4020E-4	5.4120E-4	3.4760	2.9607	3.2184
20		0	0			
30	temp30.dat	-6.4165E-4	-5.4389E-4	-3.4841	-2.9755	-3.2298
70	temp70.dat	-3.5460E-3	-3.2777E-3	-19.2545	-17.9317	-18.5931
120	temp120.dat	-1.0475E-2	-1.0692E-2	-56.8806	-58.4945	-57.6896

Table A20: F.E. results for 4 ply repair, mesh shown in Figure A6

Temp °C	G (MPa)	η_C	η_1	η_3	Loss Factor.	File
-67	300	0.004	.026	.004	0.019898	rjc01.dat
-60	300	0.004	.026	.004	0.019898	rjc01.dat
-50	300	0.004	.026	.004	0.019898	rjc01.dat
-40	300	0.004	.026	.004	0.019898	rjc01.dat
-30	300	0.004	.026	.004	0.019898	rjc01.dat
-20	300	0.004	.026	.004	0.019898	rjc01.dat
-10	300	0.004	.026	.004	0.019898	rjc01.dat
0	300	0.004	.026	.004	0.019898	rjc01.dat
10	300	0.004	.026	.004	0.019898	rjc02.dat
20	300	0.100	.026	.004	0.030599	rjc03.dat
30	280	0.170	.026	.004	0.039169	rjc04.dat
40	200	0.240	.026	.004	0.054978	rjc05.dat
50	130	0.400	.026	.004	0.096385	rjc06.dat
60	85	0.522	.026	.004	0.146113	rjc07.dat
70	50	0.677	.026	.004	0.227325	rjc08.dat
80	25	0.850	.026	.004	0.346056	rjc09.dat
90	5	1.042	.026	.004	0.409403	rjc10.dat
100	1.7	1.000	.026	.004	0.233752	rjc11.dat
110	1.0	1.000	.026	.004	0.163993	rjc12.dat
120	0.9	0.500	.026	.004	0.086328	rjc13.dat

Table A21: Strain for Dyad 609, 2a=50 mm

Temp °C	4 ply *(DR 16_e_609a.nb)	6 ply *(DR 16_e_609b.nb)	8 ply *(DR 16_e_609c.nb)
-67	152.44	152.295	159.271
-60	152.44	152.295	159.271
-50	152.44	152.295	159.271
-40	152.44	152.295	159.271
-30	152.44	152.295	159.271
-20	152.44	152.295	159.271
-10	152.44	152.295	159.271
0	152.44	152.295	159.271
10	152.44	152.295	159.271
20	128.027	114.173	104.22
30	113.193	97.0556	85.6162
40	96.4419	79.9758	68.7329
50	73.8778	59.3936	49.9203
60	61.5286	49.0792	40.9631
70	51.8775	41.4192	34.44
80	47.2442	38.0504	31.492
90	66.6844	53.5769	42.7501
100	108.418	85.979	66.9118
110	137.056	108.312	83.6649
120	190.856	151.844	117.462-

*Mathematica file is: DampedRepair16_e_609a.nb etc.

Table A22: F25_Alum.txt, (2a=50 mm crack length)

Temp °C	fmm	fbm	Fmb	fbb
-67.	0.10052	0.03248	0.008905	0.03179
-60	0.10052	0.03248	0.008905	0.03179
-50	0.10052	0.03248	0.008905	0.03179
-40	0.10052	0.03248	0.008905	0.03179
-30	0.10052	0.03248	0.008905	0.03179
-20	0.10052	0.03248	0.008905	0.03179
-10	0.10052	0.03248	0.008905	0.03179
0	0.10052	0.03248	0.008905	0.03179
10	0.10052	0.03248	0.008905	0.03179
20	0.10052	0.03248	0.008905	0.03179
30	0.10052	0.03248	0.008905	0.03179
40	0.10052	0.03248	0.008905	0.03179
50	0.10052	0.03248	0.008905	0.03179
60	0.10052	0.03248	0.008905	0.03179
70	0.10052	0.03248	0.008905	0.03179
80	0.10052	0.03248	0.008905	0.03179
90	0.10052	0.03248	0.008905	0.03179
100	0.10052	0.03248	0.008905	0.03179
110	0.10052	0.03248	0.008905	0.03179
120	0.10052	0.03248	0.008905	0.03179

Table A23: F25_Boron_c.txt , (cracklength 2a = 50 mm)

Temp °C	fmm	fbm	Fmb	fbb
-67.	0.1722	0.0732	0.0142	0.0397
-60	0.1722	0.0732	0.0142	0.0397
-50	0.1722	0.0732	0.0142	0.0397
-40	0.1722	0.0732	0.0142	0.0397
-30	0.1722	0.0732	0.0142	0.0397
-20	0.1722	0.0732	0.0142	0.0397
-10	0.1722	0.0732	0.0142	0.0397
0	0.1722	0.0732	0.0142	0.0397
10	0.1722	0.0732	0.0142	0.0397
20	0.1722	0.0732	0.0142	0.0397
30	0.1732	0.0735	0.0142	0.0399
40	0.1744	0.0738	0.0142	0.0402
50	0.1755	0.0741	0.0142	0.0404
60	0.1768	0.0745	0.0142	0.0407
70	0.1781	0.0748	0.0142	0.0409
80	0.1794	0.0752	0.0142	0.0412
90	0.1808	0.0756	0.0142	0.0415
100	0.1824	0.0760	0.0142	0.0419
110	0.1840	0.0764	0.0142	0.0422
120	0.1857	0.0769	0.0141	0.0426

Appendix B: Costs

B.1. Costs of damped repair

The costs of this type of repair to an F / A-18 aft fuselage panel are shown in Table B1. The cost of a RAAF metal scab repair are also shown as a comparison. Included are costs of materials and labour. Labour is required to prepare surfaces of the damping material and also the lay-up of the Boron, and adhesive, and placing in the auto-clave. Also the labour is involved in setting up the repair, prepare the metal surface, vacuum bagging and bonding and curing the patch on the aircraft. The size of the patch for damping repairs is usually larger than the panel in order that the cracks at the edge of the repair are covered. In this case the chemical milled panel is of dimensions 176 x 176 mm. A factor 1.25 is used to increase the patch dimension to 220 x 220 mm. These costs were based on 2006 costs. Labour to construct patch was based on costs to prepare 4 ply specimen for the flight trials. A total cost of $7000. is slightly less than the costs of $10,000. for a metallic repair used by the RAAF, which are replaced every year. The damped repair has an infinite fatigue life.

Table B1: Costing for metal scab repair and damped repair, (2006 costs)

RAAF metal scab repair		DSTO highly damped repair	
ASTFITT	20hrs for 1 person	Adhesive FM300-2K	$243
	3hrs for 2nd person	Boron	$388
ATECH	8hrs for 4 people to R & I the formation light.	Dyad 609	$152
ATECH		Construction and cure in autoclave 24hrs	$2880
ASURFIN	3hrs for 1 person to strip area and paint patch & area	Preparation 4hrs	$480
		Application 2x8hrs	$1920
		Clean, paint and repair 4hrs	$480
Total man hours	62	Total man hours	48
Assumed rate / hr	$120	Assumed rate / hr	$120
Approximate cost	$7440	Cost	$6543
Cost of heat treatment of patch and man hours	?	-	-
Cap cost at:	$10,000	Cap cost at:	$7,000
Total time	4 days	Total time	1 day
NDI	Difficult	NDI	Better NDI
Lifetime	Temporary	Lifetime	Infinite

DEFENCE SCIENCE AND TECHNOLOGY ORGANISATION
DOCUMENT CONTROL DATA

1. PRIVACY MARKING / CAVEAT (OF DOCUMENT)

2. TITLE

Generic Design Procedures for the Repair of Acoustically Damaged Panels

3. SECURITY CLASSIFICATION (FOR UNCLASSIFIED REPORTS THAT ARE LIMITED RELEASE USE (L) NEXT TO DOCUMENT CLASSIFICATION)

Document	(U)
Title	(U)
Abstract	(U)

4. AUTHOR(S)

R.J. Callinan, C.H. Wang, S. Sanderson and S.C. Galea

5. CORPORATE AUTHOR

DSTO Defence Science and Technology Organisation
506 Lorimer St
Fishermans Bend Victoria 3207 Australia

6a. DSTO NUMBER	6b. AR NUMBER	6c. TYPE OF REPORT	7. DOCUMENT DATE
DSTO-RR-0283	AR-013-231	Research Report	December 2008

8. FILE NUMBER	9. TASK NUMBER	10. TASK SPONSOR	11. NO. OF PAGES	12. NO. OF REFERENCES
M1/9/1068	04/241	DGACS	60	31

13. URL on the World Wide Web

http://www.dsto.defence.gov.au/corporate/reports/DSTO-RR-0283.pdf

14. RELEASE AUTHORITY

Chief, Air Vehicles Division

15. SECONDARY RELEASE STATEMENT OF THIS DOCUMENT

Approved for public release

OVERSEAS ENQUIRIES OUTSIDE STATED LIMITATIONS SHOULD BE REFERRED THROUGH DOCUMENT EXCHANGE, PO BOX 1500, EDINBURGH, SA 5111

16. DELIBERATE ANNOUNCEMENT

No Limitations

17. CITATION IN OTHER DOCUMENTS Yes

18. DSTO RESEARCH LIBRARY THESAURUS http://web-vic.dsto.defence.gov.au/workareas/library/resources/dsto_thesaurus.shtml

Stress intensity factors, Bonded composite repairs, Sonic fatigue, Viscoelastic damping, Power spectra, Crack growth

19. ABSTRACT

Acoustic fatigue is the result of high frequency lateral vibration of an aircraft panel due to time varying pressure waves caused by engine and/or aerodynamic effects. For example, acoustically induced cracks have been recorded in the lower external surface of the nacelle skin of the F/A-18 aircraft and aft fuselage. In the case of the inlet nacelle overall sound pressure levels of the order of 172 dB have been recorded. Attempts to repair these cracks by applying standard methods of bonded repair developed for in-plane loads were made. However, the cracks continued to grow at a similar rate. While the repair of cracked aircraft structures subjected to in-plane loads using bonded repairs has resulted in considerable aircraft life time extension and hence cost savings, the use of bonded patches to repair panels with acoustically induced cracks (acoustic fatigue) is only recent. In this report a generic design procedure is presented for the repair of panels containing acoustically induced cracks using constrained layer damping (CLD). The application of bonded repairs to acoustically-induced cracks requires analytical tools that take into account high frequency out-of-plane vibration. The analytical tools described in the report will enable the rapid design of effective repairs using closed form solutions. A potential outcome for this study could be application to the repair of the batch 11 F/A-18 aircraft which suffer from acoustic fatigue cracking on the aft fuselage. Over a period of ten years this could result in cost savings of one order of magnitude improvement over those for metallic repairs.